

8-2014

Characterization Of The New Xofter Axxent Electronic Brachytherapy Source Using Presage(Tm)

Jennifer Sierra Irwin

Follow this and additional works at: https://digitalcommons.library.tmc.edu/utgsbs_dissertations



Part of the [Medicine and Health Sciences Commons](#)

Recommended Citation

Irwin, Jennifer Sierra, "Characterization Of The New Xofter Axxent Electronic Brachytherapy Source Using Presage(Tm)" (2014). *Dissertations and Theses (Open Access)*. 503.
https://digitalcommons.library.tmc.edu/utgsbs_dissertations/503

This Thesis (MS) is brought to you for free and open access by the MD Anderson UTHealth Houston Graduate School at DigitalCommons@TMC. It has been accepted for inclusion in Dissertations and Theses (Open Access) by an authorized administrator of DigitalCommons@TMC. For more information, please contact digcommons@library.tmc.edu.

CHARACTERIZATION OF THE NEW XOFT AXXENT ELECTRONIC BRACHYTHERAPY
SOURCE USING PRESAGE™

By

Jennifer Sierra Irwin, B.S.

Approved:

Geoffrey S. Ibbott, Ph.D.
Advisory Professor

David Followill, Ph.D.

Kent Gifford, Ph.D.

Ramesh Tailor, Ph.D.

Shouhao Zhou, Ph.D.

APPROVED:

Dean, The University of Texas
Graduate School of Biomedical Sciences at Houston

CHARACTERIZATION OF THE NEW XOFT AXXENT ELECTRONIC BRACHYTHERAPY
SOURCE USING PRESAGE™

A

THESIS

Presented to the Faculty of
The University of Texas
Health Science Center at Houston
and
The University of Texas
MD Anderson Cancer Center
Graduate School of Biomedical Sciences
in Partial Fulfillment
of the Requirements
for the Degree of

SPECIALIZED MASTER OF SCIENCE

by

Jennifer Sierra Irwin, B.S.

Houston, Texas

August 2014

Dedication

To my mother, who instilled in me an appreciation and love of learning and higher education, and for always believing in me and encouraging me to do my best.

To my father, for always being a phone call or a text away and for supporting me for these past two years. I wouldn't have made it without you.

Acknowledgements

First and foremost, I would like to thank my advisor, Dr. Geoffrey Ibbott, for everything he has done for me and the time he has invested in me over the past two years. He managed to turn every mistake into a learning experience, and I was glad to always be able to count on his support. Next, I would like to thank the members of my committee – Dr. David Followill, Dr. Kent Gifford, Dr. Ramesh Tailor, and Dr. Shouhao Zhou – for the time and effort they've each invested in my project. I would also like to thank Dr. Stephen Kry for stepping up to be a substitute committee member. I would like to acknowledge Dr. John Adamovics for manufacturing the numerous dosimeters I needed for this project. Furthermore, I would like to thank Dr. Slade Klawikowski for always being available and willing to assist me and brainstorm with me, as well as for teaching me about PRESAGE™ and the DMOS system. I would like to thank Ryan Grant, M.S., for her expert advice concerning PRESAGE and DMOS during the troubleshooting phase of my project; her assistance and assurances were invaluable. As for the remainder of our lab group – Mitchell Carroll, M.S., Yvonne Roed, Hannah Lee, Mamdooh Alqathami, and Dr. Jihong Wang – thank you for listening and for all your helpful suggestions along the way. I would like to thank Tom Rusch at Xoft, a subsidiary of iCAD, for providing the sources used in this experiment. I extend a hearty thanks to the people at the University of Wisconsin ADCL, specifically to John Micka and Samantha Simiele, for being so welcoming and helpful during my brief visit there to make Xoft irradiations using their system. Finally, I would like to thank the people at the MD Anderson Cancer Center ADCL, specifically Nina Garcia-Gutierrez, for her assistance, laughter, and teaching me how to use the HDR system there.

CHARACTERIZATION OF THE NEW XOFT AXXENT ELECTRONIC BRACHYTHERAPY SOURCE USING PRESAGE™

Jennifer Sierra Irwin, B.S.

Advisory Professor: Geoffrey S. Ibbott, Ph.D.

With continuing advances in the burgeoning field of electronic brachytherapy, an accurate method of 3D dosimetry is needed to ensure understanding of dose distributions, which can improve patient care. The aim of this study was to characterize the Xofter Axxent electronic brachytherapy source using PRESAGE™ dosimeters in order to obtain independent confirmation of TG-43U1 dosimetry values, as well as to further add to the literature of both Xofter and PRESAGE.

PRESAGE is a polyurethane-based solid 3D dosimeter doped with a radiochromic leuco dye which produces a linear change in optical density when exposed to radiation. This optical density change is imaged using an optical-CT scanner and reconstructed for analysis using MATLAB software. A Xofter source with a measured air kerma strength of 126095 U was used in this experiment to irradiate 8 PRESAGE dosimeters to 15 Gy at 1 cm in order to evaluate the dose rates from $r=1$ cm to $r=5$ cm. The dosimetric parameters were calculated and compared to the Rivard et al. (1)(1) parameters.

In general, the measured results closer to the source more closely matched the comparison data than those values measured further from the source. The radial dose function was within 6% of the expected values, and the anisotropy function, ignoring the extreme outlier at each radius, was within 35% of the expected values. An incorrect shutter value was used when imaging the dosimeters so that the post-irradiation scans were repeated 2 months after the irradiation, allowing time for the dosimeter to darken as it aged, which increased background noise, and time for the dose signal to fade, thereby bringing the dose signal closer to the background noise. The experiment should be repeated to obtain more accurate results.

Table of Contents

Signature Page	i
Title Page	ii
Dedication	iii
Acknowledgements	iv
Abstract	v
Table of Contents	vi
List of Figures	viii
List of Tables.....	ix
Chapter 1 Introduction.....	1
1.1 Statement of Problem	1
1.1.1 General Problem Area.....	1
1.1.2 Specific Problem Area.....	1
1.2 Background	2
1.2.1 Brachytherapy	2
1.2.2 Electronic brachytherapy.....	4
1.2.2.1 Xofter.....	4
1.2.2.2 Previous Xofter Studies	8
1.2.3 PRESAGE Dosimeters.....	8
1.2.3.1 Gel Dosimetry	8
1.2.3.2 Characteristics of PRESAGE Dosimeters	9
1.2.3.3 Drawbacks of PRESAGE	11
1.2.3.4 Optical-CT Imaging with DMOS	11
1.2.3.5 Previous work with PRESAGE	15
1.3 Hypothesis and Specific Aims.....	16
Chapter 2 Methods & Materials	16
2.1 Dosimeter Design	16
2.2 Treatment setup and delivery	18
2.2.1 Dose calibration	18
2.2.2 Pre-irradiation.....	20
2.2.3 Treatment delivery	21

2.3 Imaging and analysis	24
2.3.1 Optical-CT imaging	24
2.3.2 Data Acquisition in MATLAB	25
2.3.2.1 Testing the code	28
2.4 TG-43U1 Formalism	29
2.4.1 Air kerma strength	29
2.4.2 Air kerma rate calibration	30
2.4.3 Dose rate	30
2.4.4 Dose rate constant	31
2.4.5 Geometry function	31
2.4.6 Anisotropy function	32
2.4.7 Radial Dose Function	33
Chapter 3 Results for Xofig Source	34
3.1 Soft Dosimeter Batch	34
3.2 Radial dose function	35
3.3 Anisotropy function	36
Chapter 4 Discussion	40
4.1 Concentric Rings Artifact	40
4.2 Solution to Remove the Artifact	44
4.2.1 Dose Rate and Dose Rate Constant	46
Chapter 5 Uncertainty Analysis	46
5.1 Anisotropy function	47
5.2 Radial dose function	47
Chapter 6 Conclusion	47
Appendix A	48
Appendix B	51
Appendix C	55
References	56
Vita	61

List of Figures

Figure 1. Figure 1. Xofter Axxent source in its shipment box	5
Figure 2. Drawing of inside the Xofter catheter.(1)	5
Figure 3. Xofter Axxent electronic brachytherapy system controller (24)	6
Figure 4. Example of an irradiated solid 1 kg PRESAGE dosimeter	10
Figure 5. Diagram of DMOS system's main components	12
Figure 6. Screenshot of DMOS Acquisition GUI without a dosimeter in the tank	13
Figure 7. Screenshot of the DMOS Reconstruction GUI.....	15
Figure 8. PRESAGE with 1.5 cm diameter large channel (soft batch)	17
Figure 9. PRESAGE with 5.3 mm small channel (hard batch)	17
Figure 10. Irradiated plug for large channel dosimeters.....	17
Figure 11. PRESAGE cuvettes for dose calibration.....	18
Figure 12. Cuvette irradiation setup (7)	19
Figure 13. Hard dosimeters dose response curve	20
Figure 14. Soft dosimeters dose response curve	20
Figure 15. MTF at UWADCL	22
Figure 16. Dosimeter shielded from light and surrounded by rice in phantom.....	23
Figure 17. Xofter Axxent source inside plug inside PRESAGE dosimeter.....	24
Figure 18. Diagram of the transverse plane in the PRESAGE dosimeter	26
Figure 19. Top view of the dosimeter showing the annulus described	27
Figure 20. Screenshot of PhoenixFire GUI, showing z slice where anode is located	28
Figure 21. Modified TG-43U1 coordinate system for brachytherapy dose calculations	29
Figure 22. Prescan and postscan images of a soft dosimeter with a large channel	35
Figure 23. Graphical comparison of the radial dose function	36
Figure 24. Anisotropy function for $r=2\text{cm}$	40
Figure 25. Anisotropy function for $r=3\text{cm}$	40
Figure 26. Reconstructed image showing the concentric ring artifact	41
Figure 27. Pre- and post-irradiation scans of four different dosimeters.....	42
Figure 28. Projection images with large delta	43
Figure 29. The extent of the available data	44
Figure 30. Projection images with normal delta	45
Figure 31. Final post-irradiation scan of a dosimeter showing no ring artifact.....	45
Figure 32. Example background level plot.....	46

List of Tables

Table 1. Dose rate categories from ICRU Report 38 (16)	2
Table 2. Common brachytherapy radionuclides and their characteristics (14, 15)	3
Table 3. Dose rate constant (24)	31
Table 4. Geometry factors for a point source.....	32
Table 5. Measured anisotropy function at 50 kV (1)	33
Table 6. Radial dose function values measured at 50 kV (1).....	33
Table 7. Radial Dose Function Comparison	36
Table 8. Anisotropy function measured in PRESAGE	37
Table 9. Anisotropy function: Percent Error	38
Table 10. PRESAGE Anisotropy function: Standard Deviation	39
Table 11. PRESAGE Anisotropy Function: Percent Coefficient of Variance	39
Table 12. Uncertainty in PRESAGE measurement of Dose Rate	47

1 Introduction

1.1 Statement of Problem

1.1.1 General Problem Area

With advances in radiotherapy technology leading to the delivery of more conformal doses to smaller treatment volumes (2, 3), quality assurance (QA) of such delivery and equipment has become more important. Currently, 1D and 2D QA methods are used to sample dosimetric data in 3D volumes. Dosimetry is performed so the radiation dose given to a patient can be accurately measured, but this is innately a 3D problem, wherein the radiation interacts with atoms within the patient's body in all directions, and should therefore have a 3D method of measurement. 1D and 2D systems have been used effectively, but can have volume average, artifacts, and energy dependence. The advantage of 3D dosimetry is that a complete dose distribution can potentially be measured in a single irradiation; this is impractical for TLD irradiations, and film only provides one plane at a time. 3D dosimetry can conceivably save the physicist valuable time.

The need for a 3D dosimeter is accentuated when considering brachytherapy, or short range therapy, where small radioactive sources are placed directly within the treatment site, creating sharp dose fall-off regions. The dose in these regions is difficult to measure accurately using conventional dosimetry systems. For example, it is difficult to accurately measure steep dose gradients using 1D dosimeters such as thermoluminescence dosimeters, due to their finite size and volume-averaging effects(4); and some 2D dosimeters such as film are subject to artifacts from handling, dependence on energy, and possibly dependence on dose rate (at the extrema of dose and dose rate) (5). Dose measurements are required to characterize brachytherapy sources for patient treatment-planning calculations.

1.1.2 Specific Problem Area

PRESAGE™ is a new type of 3D dosimeter which addresses some of the problems of 1D and 2D dosimeters(6) mentioned above. PRESAGE has been used to determine dose distributions from a linear accelerator(6), low dose rate (LDR) brachytherapy sources(7), as well as high dose rate (HDR) brachytherapy sources(8).

In the last decade, a new electronic brachytherapy source, Xofter Axxent (Xofter, Inc., a subsidiary of iCAD, San Jose, CA) has been studied for use in partial breast irradiation (PBI) treatments for breast cancer. Xofter has also been studied for use in skin treatments and in vaginal cancer treatments as a replacement for ^{192}Ir (9). Although many Xofter applications have been studied since its introduction (10-12), there is only one published

paper that provides TG-43U1 dosimetry data for the source (1). PRESAGE has not yet been used to characterize this new HDR system.

1.2 Background

1.2.1 Brachytherapy

Brachytherapy, or short range radiotherapy, is a method of radiation treatment wherein a radioactive source is placed in or near a tumor and the radiation from the decaying source causes damage to the tumor cells, often while sparing more surrounding normal tissue than external beam radiotherapy (13). Generally, brachytherapy uses sealed radioactive sources, radioactive material encapsulated within a metal wall, to deliver this form of treatment. It can be delivered interstitially, inside a cavity (intracavitary), or to the surface of a patient. Cancers that are commonly treated with brachytherapy are skin, breast, prostate, vaginal, cervix, and eye.(14)

There are advantages to brachytherapy over external beam radiotherapy. First, brachytherapy involves placement of sources in or close to the target tissue, maximizing the tumor dose and minimizing the dose to surrounding normal tissue. Second, brachytherapy has a lower dose rate when compared to external beam radiotherapy. The lower dose rate can be exploited, as will be explained below.

Brachytherapy was first performed with radium sources, and later, radon, cobalt, tantalum, gold, and americium. Today, these sources have been replaced by cesium, iodine, iridium, and palladium (15). Brachytherapy, using the various isotopes, will either be classified as low dose rate (LDR) or high dose rate (HDR) depending on the ICRU definition. The International Commission on Radiation Units (ICRU) and Measurements Report 38 (16) defines three main categories of dose rate: high, medium, and low, as described in Table 1.

Dose Rate Category	Dose Rate (Gy/hr)
Low Dose Rate (LDR)	.04 - 2
Medium Dose Rate (MDR)	2 - 12
High Dose Rate (HDR)	>12

Table 1. Dose rate categories from ICRU Report 38 (16)

Table 2 contains the most commonly used radioisotopes in each dose rate category, along with their dose rate, half-life, and gamma-ray energy range.

Isotope	Dose Rate	Half-life	γ-ray Energy
²⁴¹ Am	LDR	432.2 years	13.9-59.5 keV
¹³⁷ Cs	HDR/LDR	30.0 years	662 keV
⁶⁰ Co	HDR/LDR	5.26 years	1.17-1.33 MeV
¹⁹⁸ Au	LDR	2.7 days	0.41-1.09 MeV
¹²⁵ I	LDR	59.4 days	35.5 keV
¹⁹² Ir	HDR/LDR	73.8 days	0.14-1.06 MeV
¹⁰³ Pd	LDR	17.0 days	20-22.7 keV
²²⁶ Ra	LDR	1622 years	0.05-2.4 MeV
²²² Rn	LDR	3.83 days	0.05-2.4 MeV
¹⁸² Ta	LDR	115 days	0.04-1.45 MeV

Table 2. Common brachytherapy radionuclides and their characteristics (14, 15)

LDR brachytherapy involves placement of sources within or adjacent to the tumor for an extended period of time, often several days and in some cases, permanently. The low dose rate allows normal tissue to perform repair during the treatment, in contrast with fractionated external beam therapy where repair takes place between treatment fractions. At the same time, however, the continuous dose delivery allows the total dose, or a large fraction of the dose, to be delivered in a shorter elapsed time, thereby minimizing tumor repopulation effects.

In contrast, HDR brachytherapy combines the shorter overall treatment time and dose localization capabilities of LDR brachytherapy with the benefits of hypofractionated external beam therapy. With HDR, normal cells have time between treatment fractions to repair sublethal damage. (13)

AAPM TG-43U1(17) discusses how to calculate the dose from brachytherapy sources, and AAPM TG-56 (18) discusses how to calibrate brachytherapy sources. TG-43U1 will be discussed in detail in Chapter 2, and TG-56 will be briefly explained here for the most common HDR source, ¹⁹²Ir. The HDR iridium source has no national standard; however, an interpolation can be made between ¹³⁷Cs and orthovoltage energies. As an interim standard, the interpolative free air secondary standard method is now accepted. (19) To perform this calibration, air kerma rate measurements are taken along the z-axis of the source from 10 to 100 cm away with an ion chamber in a free air geometry. (Section 2.4 and Figure 21 provide a detailed description of the TG-43U1-defined coordinate system.) The ion chamber should have a buildup cap thick enough to ensure secondary electron

equilibrium. The ^{192}Ir air kerma calibration factor is derived by interpolating between the ^{137}Cs and orthovoltage air kerma factors, which are Accredited Dosimetry Calibration Laboratory (ADCL) or National Standards Institute of Technology (NIST) traceable. It should be noted that this calibration procedure is not recommended to be performed by clinical medical physicists, but rather by the trained calibration laboratory personnel. This procedure is only noted here for comparison with the Xofter Axxent calibration procedure.

Both AAPM TG-56 and AAPM TG-59 (20) discuss how to perform a standard HDR treatment. This is discussed here very generally, again, for comparison with a Xofter Axxent electronic brachytherapy treatment. An HDR source is at the end of a long wire, which is kept within the shielded afterloader. The patient is setup with the catheter in place, within the appropriate applicator, as is applicable to the treatment. The personnel leave the room and operate the afterloader from outside the treatment vault. When the treatment begins, the source, on its wire, moves out of the afterloader and down into the catheter, and into the patient. Various dwell positions and dwell times of the HDR source, as determined with the treatment planning system (TPS) to achieve the desired dose to the tumor, are controlled by the HDR console during treatment.

1.2.2 Electronic brachytherapy

In response to complicated intraoperative radiotherapy procedures and requirements, as well as the inconvenience of dealing with radioactive materials regulations and security requirements, small, mobile, low kV x-ray sources were developed in the late 1990s. (21) These sources have since been co-opted by the brachytherapy community. Their low energy x-rays greatly minimized exposure to the staff, though their usage is currently limited to small tumors. The Xofter Axxent system was ostensibly developed to mimic the treatment energies of HDR ^{192}Ir so it could be directly substituted into many current cancer treatment techniques.

AAPM TG-61 (22) covers low energy x-ray calibration and dosimetry. This is typically used for superficial and orthovoltage machines, but, the Xofter User's Manual (22) states that it should be applied in the interim while an AAPM task group report is being prepared on electronic brachytherapy. Low kV x-ray calibrations should be traceable to a national standard, either NIST or an ADCL, and are performed in air, to obtain the air kerma strength.

1.2.2.1 Xofter

Xofter Axxent is an electronic brachytherapy system that consists of an electronic controller, a miniature electronic x-ray source inside a flexible catheter (shown in Figure 1),

and a balloon applicator. The x-ray tube inside the catheter is water-cooled with sterile water; the x-ray tube inside the catheter is shown in Figure 2. The catheter is 250 mm in length and 5.1-5.4 mm in diameter. (23)

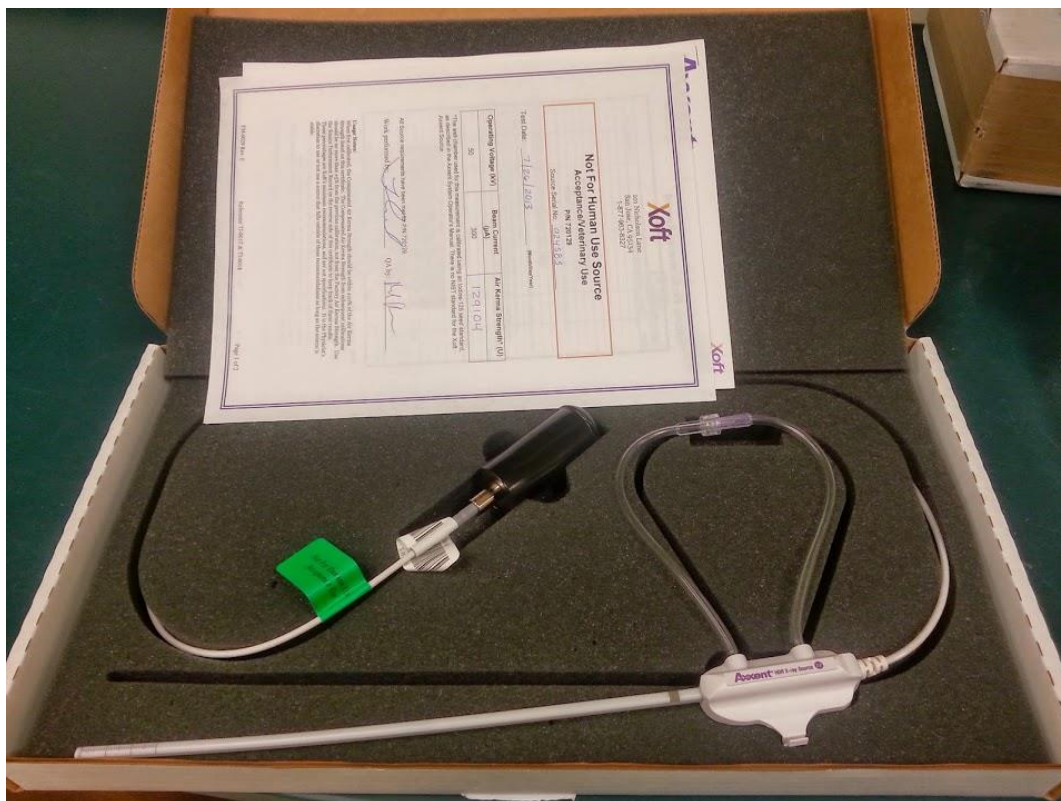


Figure 1. Xoft Axxent source in its shipment box.

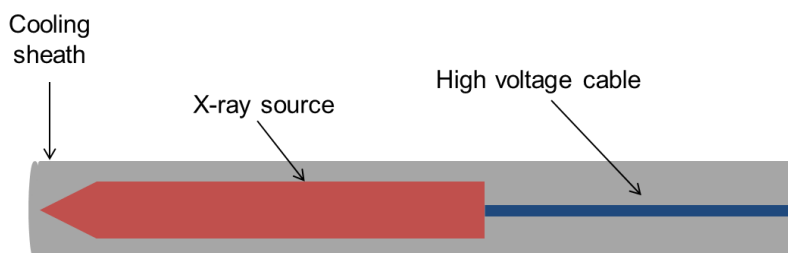


Figure 2. Drawing of inside the Xoft catheter.(1)

The Xofter source can deliver dose at voltages of 40 kV, 45 kV, and 50 kV. The average energy of the Xofter spectrum at 50 kV is 26.6-26.7 keV. The dose rate is expected to be 0.6 Gy/min at 3 cm from the source axis.

The power requirement for the Xofter Axxent device is 15 W. The maximum beam current is 300 μA , but is adjustable for treatment. The x-ray tube can be stepped to different

dwell positions within the catheter at millimeter intervals and for different dwell times, just as conventional HDR sources can be. The manufacturer recommends that each Xofter source is disposed of after whichever of the following occurs first: 10 fractions, 170 minutes of treatment time, or 35 days after the initial calibration, provided the cooling water is vacuumed out after each use. (24) All sources are disposable. The Xofter system complies with the International Electrotechnical Commission (IEC) medical electrical safety equipment standard 60601-2-17. (25)

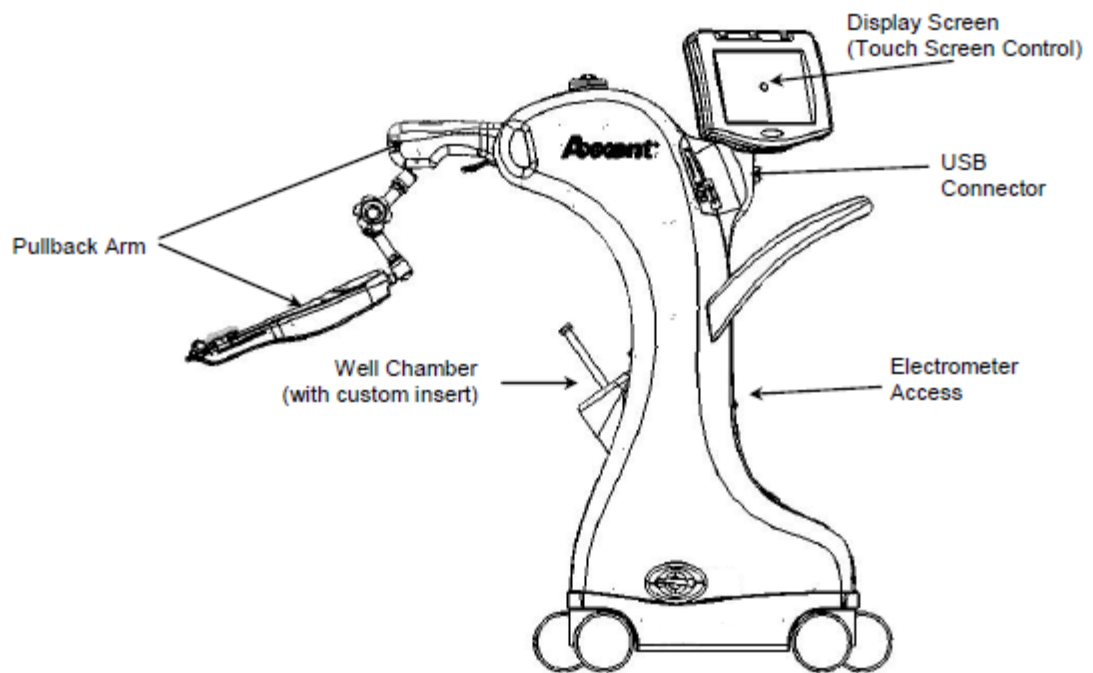


Figure 3. Xofter Axxent electronic brachytherapy system controller (24)

Both BrachyVision and Plato TPS have been verified for use with the Xofter Axxent electronic brachytherapy source. If an electrical malfunction occurs during the treatment, as mandated by the IEC (25), the controller, shown in Figure 3, will stop the treatment and record the treatment values at that time. The display shows dwell position, and total planned time, elapsed time, and time left at current dwell position; the display screen, as part of the system controller, is shown in Figure 3.

Air kerma strength is measured by the manufacturer prior to shipment, and again by the physicist prior to each fraction. Before each clinical treatment, the air kerma strength of the source is measured and compared to the “nominal” air kerma strength, which was determined when the system was initially calibrated and is used to create treatment plans. A ratio of the “nominal” to the measured air kerma strength is used to adjust the dwell times

in the TPS. The air kerma strength is measured in the attached Standard Imaging well chamber and electrometer (Models HDR 1000 Plus and MAX-4000, respectively (Standard Imaging, Middleton, WI)) using a custom insert that attenuates the source. The purpose of this insert is threefold: 1) it shields the source so personnel may remain in the treatment room while calibrating, 2) it absorbs the lower energy photons that would be absorbed in the applicator during treatment, and 3) it reduces the source output so it is within the operating range of the electrometer. This well chamber, insert, and electrometer system must be calibrated by an ADCL every two years.

The well chamber calibration for this source has no NIST standard procedure; however, the ADCL at the University of Wisconsin (UW) developed a secondary calibration method combining methodology described in both TG-43U1 and TG-61 (Report 79) on low energy x-ray dosimetry. The calibration coefficient for the well chamber is based on a comparison of the I-125 national standard and the measurement of the Xofter Axxent source using an Attix free-air chamber (FAC) at the UWADCL (University of Wisconsin Accredited Dosimetry Calibration Laboratory). First, a well chamber calibration coefficient C is obtained for I-125, resulting in air kerma strength per corrected well chamber current unit (U/A). Next, the output of the Xofter source is measured in the FAC, and then in the well chamber; a calibration coefficient is obtained for Xofter. The ratio R is defined as the ratio of the Xofter calibration coefficient to C , the I-125 well chamber calibration coefficient. C times R results in N_{SK} , or the air kerma strength well chamber calibration coefficient for Xofter. This is the “nominal” S_K used in the TPS; S_K is air kerma strength in U , and its full TG-43U1 definition is provided in Chapter 2. The manual describes a “compensated” air kerma strength value, which is the air kerma strength corrected for temperature and pressure. (24)

Each patient receives their own disposable Xofter source. To deliver a treatment, the source is connected to the high voltage and water-cooling systems, calibrated in the well chamber, then finally inserted into the applicator in the patient. The operator may stay in the room during the treatment, due to the low energy nature of the x-rays produced by the Xofter source. This is an advantage to treating with Xofter. For example, for a breast cancer treatment, a 0.4 mm lead equivalent shield placed over the patient’s breast will reduce exposure from 15 mR/h to 1 mR/h at the operator’s location. However, the resulting scattered radiation will increase the dose to the patient. To further reduce exposure, personnel may wear lead-equivalent aprons. This also drastically reduces the room shielding requirements. (23)

TG-152 (publication date unknown) has been assigned to address clinical application and quality assurance procedures for electronic brachytherapy sources, including the Xofter Axxent system.

1.2.2.2 Previous Xofter Studies

Xofter has been studied as an alternative accelerated partial breast irradiation (APBI) method (10, 26), in nonmelanoma skin cancer treatment (12), and in endometrial cancer treatment (10). These studies were performed to compare Xofter with the current accepted treatment method, the ^{192}Ir HDR source, in effectiveness and dose coverage. There have been poster displays describing the Xofter dosimetry as determined using MOSFET(27), film (28, 29), ion chambers(29), an x-ray spectrometer(29), and solid and liquid water (30), as well as Monte Carlo simulations (30-32), but the Rivard et al. paper (1) is the only published source that provides the TG-43U1 dosimetry parameters. It should be noted that these posters were all done in part by a Xofter employee, and so technically violate the TG-43U1 recommendation that “independent and redundant dosimetric characterizations” be performed for every new brachytherapy source intended for clinical use.

Rivard et al. used both Monte Carlo simulations and liquid water measurements with a PTW parallel plate ionization chamber to characterize the source. The Monte Carlo simulations were based on the MCNP5 code and the EPDL97-based mcplib04 cross-section library. TG-43U1 parameters (radial dose function, anisotropy function) were determined for radial distances between 0.4 cm and 15 cm, and angles between 0° and 175°. Ion chamber measurements were made many locations corresponding to the calculation points. Operating voltages of 40 kV, 45 kV and 50 kV were used for simulations and measurements. The Rivard et al. data was used to create the Xofter User’s Manual. Characterizing the Xofter source with PRESAGE is a novel experiment, and would add independently-derived dosimetry data to the existing body of knowledge. A better understanding of Xofter dosimetry can be used to more accurately treat patients.

1.2.3 PRESAGE Dosimeters

1.2.3.1 Gel Dosimetry

PRESAGE (Heuris Pharma LLC) was introduced in 2003 as an alternative to gel dosimeters. Gel dosimetry was first explored in the 1950s; the first radiosensitive gels were doped with a dye and would change color due to a chemical reaction when exposed to radiation. The next type of gel dosimeter was doped with chloral hydrate, which reacted to radiation; the change in the gel could be observed using pH probe measurements or

spectrophotometry. In the 1980s, the chemical reaction to radiation in Fricke gels, which were doped with ferrous sulfate, could be imaged with an MRI machine.

Another type of gel dosimeter, now more common, is the polymer gel dosimeter, which would polymerize as a function of dose when exposed to radiation. The polymerization could be measured using MRI, optical-CT, x-ray CT, or ultrasound. BANANA (made of bis-acrylamide in an aqueous agarose matrix, nitrous oxide, and agarose) and BANG (made of bis-acrylamide in an aqueous agarose matrix, nitrogen, and aqueous gelatin) gels are examples of polymer gels. The optical-CT scanner developed for use with these gels was a precursor to the optical-CT scanner used in this project. (33)

There are drawbacks to using gel dosimeters. First, they are oxygen-sensitive; oxygen inhibits the polymerization process. Polymer gels must be manufactured and stored in an oxygen-free environment, which is not practical in a clinical setting. Next, gels must be stored in a container, but imaging the container results in edge artifacts, even when steps are taken to minimize these effects via refractive index matching fluid. In Fricke gels, diffusion of the ions caused a loss of spatial resolution and an unstable dose distribution. Other types of gels do not have the same diffusion issue. Lastly, when using optical-CT to image gel dosimeters, light scatter artifacts become an issue. PRESAGE addresses these issues, as explained in the next section. (34)

1.2.3.2 Characteristics of PRESAGE 3D Dosimeters

When exposed to radiation, PRESAGE dosimeters produce an optical density change that can be imaged with an optical-CT to determine dose. A PRESAGE dosimeter, as seen in Figure 4, is a polyurethane-based dosimeter that is doped with leucomalachite green (LMG) dye which reacts linearly to radiation dose, regardless of photon energy and dose rate. (6) Halocarbon free radical initiators respond to high energy radiation, and in so doing, oxidize the LMG, creating the change in OD. The sensitivity of the dosimeter depends on the type of halogens used in the initiator. (35) The oxidation of the LMG dye creates a stable signal in PRESAGE. However, some current experimental formulations of PRESAGE are attempting to create a reusable dosimeter and so do not allow a lasting stable signal. Different PRESAGE formulations are made to be more sensitive to different types of radiation, e.g., photons versus protons.

-



Figure 4. Example of an irradiated solid 1 kg PRESAGE dosimeter.

PRESAGE was created so the user can acquire a 3D volume of data from a single irradiation. PRESAGE is imaged using an optical-CT scanner, which provides the user with the optical density changes in the dosimeter which are used to determine dose. (6) The resolution of PRESAGE depends on the resolution of the scanner used to image it (see section 1.2.3.2 for more information). Its effective Z is ~ 7.7 , which closely mimics that of soft tissue or water ($Z_{\text{eff}} \sim 7.4$, in both cases). The density of PRESAGE is 1.05 g/cm^3 , which compares well with that of water. (36) PRESAGE, unlike gel dosimeters, is not oxygen sensitive and requires no external container. With PRESAGE, there is no diffusion of the dye, and it can be synthesized into different shapes and sizes. PRESAGE is, however, light and heat sensitive.

Although PRESAGE is currently best used as a relative dosimeter, an absolute dose calibration curve can be created for each batch of PRESAGE using cuvettes containing the PRESAGE material. The cuvettes are irradiated to a range of doses, then the optical density (OD) is read out. A graph of OD change versus dose in Gy is created and can be used to scale the larger PRESAGE dosimeters from that batch to an absolute dose. The calibration curve illustrates that the change in OD is linear with dose. The calibration curve can account for signal changes post-irradiation; it has been shown that the “standard” formulation signal can fade by 4% per 24-hour post-irradiation period. (6) With a slightly

different formulation (the “soft” batch), this signal fading can be accelerated, so that a dosimeter would be bleached and reusable after a week. Current research in this direction is ongoing.

1.2.3.3 Drawbacks of PRESAGE

PRESAGE is sensitive to UV and blue light (35). To prevent this sensitivity, PRESAGE is stored in black, light-tight bags when not in use. Scanning and irradiating is performed with the lights out. PRESAGE is also sensitive to temperature. This issue is dealt with by storing PRESAGE in a refrigerator kept at 4° C. For the entire pre-irradiation scan, irradiation, post-irradiation scan process, it is recommended that the PRESAGE be kept at room temperature for accurate dosimetry. (6, 37)

1.2.3.4 Optical-CT Imaging with DMOS

The optical-CT scanner used at the Imaging and Radiation Oncology Core in Houston (IROC-Houston, formerly the Radiological Physics Center (RPC)) is called DMOS (Duke Medium-field-of-view optical-CT scanner) and it is shown in Figure 5. The configuration of the scanner is as follows: a diffuse red LED light shines through the dosimeter, which is placed in an indexing tank, and on through a lens into a CCD camera. The aquarium is filled with a mix of octyl salicylate, octyl cinnamate, and light mineral oil to match the refractive index of the dosimeter at the fluid-dosimeter interfaces; this helps prevent dosimeter edge effects that blur the optical density signal. (38) The LMG dye used in PRESAGE was chosen, in part, because its visible absorbance maximum corresponds to the 633 nm red laser light that was used to optically scan PRESAGE in the first commercially-available optical-CT scanner. (6) The DMOS has a red LED light of the same wavelength.

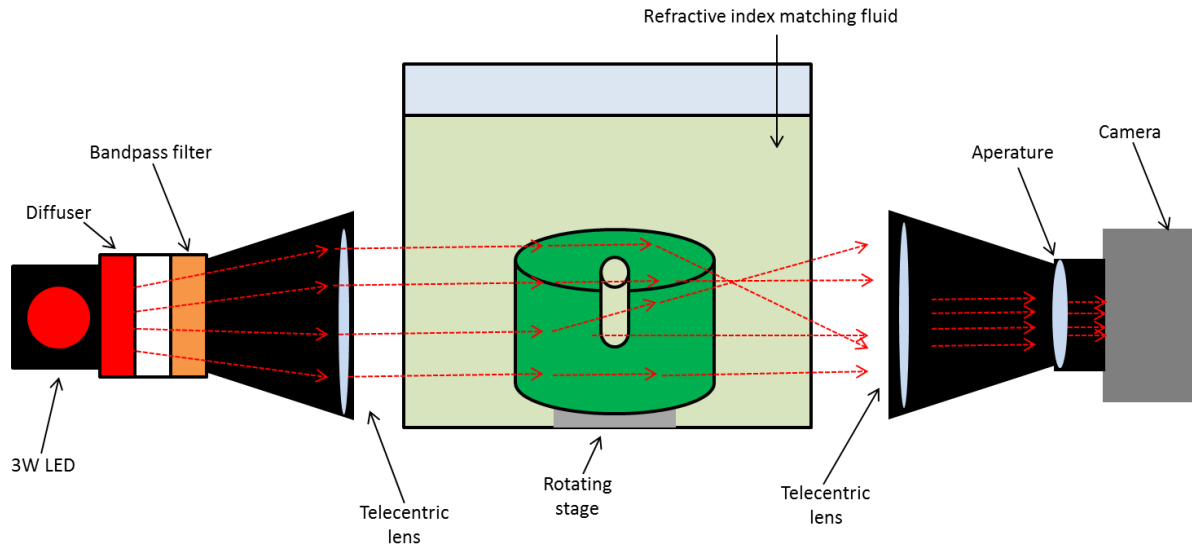


Figure 5. Diagram of DMOS system's main components.

The dosimeter rotates via an electronic stepper motor base. The lens rejects stray light that is further than 0.1° off the optical axis. The camera takes line integrals at each projection angle, which are used to reconstruct a 3D image via filtered backprojection. LabView is used to collect the images and rotate the dosimeter. An example of the DMOS Acquisition GUI (Duke University, NC) is shown in Figure 6. The user enters the filename stem, the file destination, and the scanning parameters. (39) The total scan time for a 1 kg dosimeter is between 15 and 20 minutes. This is a vast improvement on the first commercially available optical-CT scanner mentioned previously, which took 7 minutes per z slice, for a total scan time of a few hours. (40)

Dosimeters are scanned prior to and after irradiation so that background and final OD can be determined. In general, 720 projection images are taken, one every 0.5° ; 8 images are averaged together at each projection angle. A flood image is taken without a PRESAGE dosimeter in the aquarium to correct for inhomogeneities in both the matching fluid and LED light field. A dark image is taken to correct for electronic noise. Both the flood and dark images are 200 averages of one projection image.

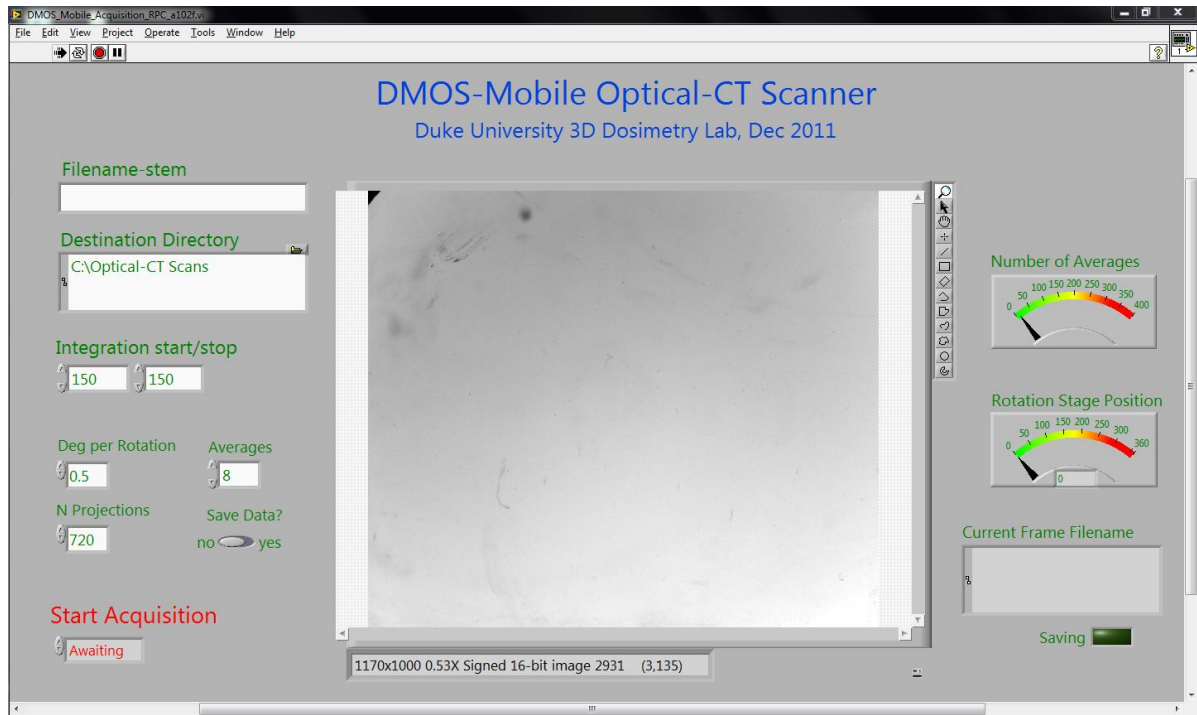


Figure 6. Screenshot of DMOS Acquisition GUI without a dosimeter in the tank.

The spatial resolution of the system depends on user settings and available storage space for the projection images. Typically, the dosimeters at IROC-Houston are scanned to have either 0.5 mm or 1 mm voxels. The resolution of PRESAGE can only be as high as the resolution of the scanner used to image it. The CCD Basler camera captures 12-bit monochromatic 1040x1392 pixel arrays.

Monochromatic light attenuates exponentially under narrow beam conditions, as exist in the DMOS. The optical-CT readout of a dose response in PRESAGE is explained by this 2D, i.e., per projection angle, equation:

$$I(x) = I_0 e^{-\int \mu(x,y) dy} \quad \text{Eqn. 1}$$

Here, I_0 is the incident intensity of the light hitting the dosimeter, $I(x)$ is the intensity of the light exiting the dosimeter at position x , and $\mu(x, y)$ is the optical attenuation coefficient per unit length. (33) From this equation, we can calculate the OD, or absorbance, of the dosimeter with this equation:

$$OD = -\log\left(\frac{I}{I_0}\right) \quad (7) \quad \text{Eqn. 2}$$

This is what is calculated and saved in the 3D data cube matrix output from the Reconstruction software. From the OD, the dose can be calculated, either by the cuvette calibration curve, or the following equation:

$$Dose = -\frac{OD}{s \times x} \quad \text{Eqn. 3}$$

where OD is defined previously, s is the sensitivity ($\Delta OD/\text{Gy}/\text{cm}$) and x is the irradiated path length in cm. If relative dose is all that is needed, the data cube is normalized to a user-specified dose delivered at a user-specified location.

Reconstruction of the projection images is completed using the DMOS software; a screenshot of the Reconstruction GUI is shown in Figure 7. First, the pre-irradiation and post-irradiation optical-CT scan images are each loaded together with a flood image and a dark image to make the corresponding corrections for background noise. To create the sinogram, a 5x5 kernel median filter is applied to reduce noise, and a 1 mm voxel size is selected for reconstruction. As part of this process, the pre-irradiation scan image is subtracted from the post-irradiation scan image to obtain a net change in the dosimeter. In the end, a series of 2D sinograms is generated.

A sinogram is a single image of all the raw data acquired by the CT scanner; an example sinogram can be seen in the top right corner of Figure 8. The horizontal axis of the sinogram represents each angle at which a projection image was taken; for this experiment, a projection image was taken every 0.5° from 0° to 360° . The vertical axis of the sinogram represents the projection images taken; 720 projection images were taken in this experiment. Filtered backprojection (FBP) is an iterative reconstruction technique which uses the sinogram to reconstruct a 3D tomographic image of the original scanned object; it is the “computed” in CT’s computed tomography.

To perform FBP, the backprojection is completed first. Backprojection reverses the image acquisition steps, taking the linear optical attenuation coefficient μ for each projection, and “smearing” it back along the angle at which the projection image was taken into its position in an empty image matrix; backprojection will fill the image matrix. In this manner, the high attenuation areas reinforce each other, as do the low attenuation areas, creating a 3D reconstructed image representation of the original object scanned. A filter is applied to correct the $1/r$ blurring caused by reconstructing an image using backprojection.(41)

The DMOS Reconstruction GUI, seen in Figure 7, reconstructs the final 3D optical-CT image of the dosimeter via filtered backprojection; the “iradon” function in MATLAB performs the backprojection, and the RAM LAK filter smoothes out the blurriness (42). The user selects the center of rotation (COR) to reconstruct around, and the size of the data cube in mm, which should be slightly larger than the physical dosimeter size. The final 3D

“image” is saved as a data cube, which is the input for the radial and anisotropy data extraction scripts. (39)

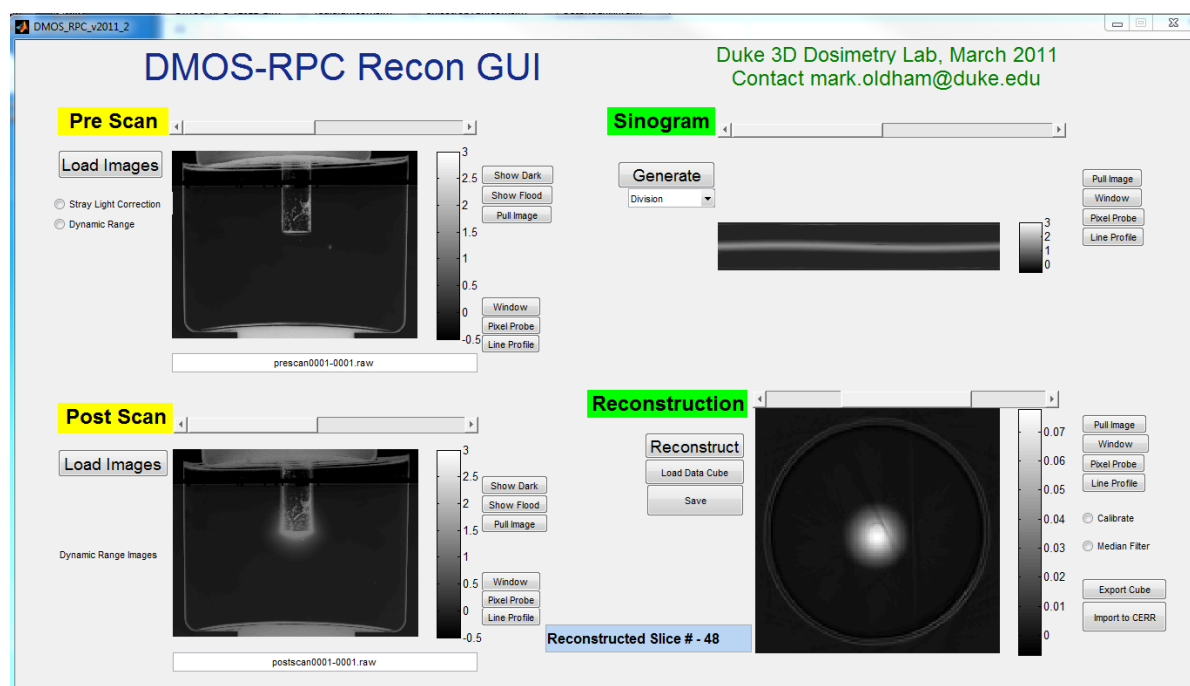


Figure 7. Screenshot of the DMOS Reconstruction GUI.

1.2.3.5 Previous work with PRESAGE

PRESAGE has been used to check IMRT dose distributions, and was found to be accurate to within 3%/3mm when evaluating dose distributions using the gamma index. (43) A gamma index comparison between EBT film, PRESAGE, and software-calculated dose distributions found three-way agreement to be within 4%/4mm. (40) An investigation of PRESAGE to measure doses in the RPC head and neck (H&N) phantom yielded acceptable results; a gamma index comparison between Eclipse, PRESAGE, and EBT was within 4%/4mm for that experiment (44). PRESAGE has been investigated for use with radiosurgery treatment systems; Niebanck found less than 3% standard deviation of dose in the target (3) and Clift et al. measured scatter factors in PRESAGE that agreed with ion chamber measurements within 4% for every field (45). PRESAGE has also been investigated as a new way to perform IMRT QA, with a 94.9% passing rate for a 3%/2mm gamma index. (46) PRESAGE was used to obtain TG-43 dosimetric parameters for the ¹⁹²Ir source, with a percentage of standard deviation between PRESAGE and published results

of 2.6% or less. (8) This will be the first time PRESAGE has been used to characterize an electronic brachytherapy source.

1.3 Hypothesis and Specific Aims

We hypothesize that PRESAGE dosimeters can measure, with 95% confidence, the AAPM TG-43U1 dosimetric parameters of the Xofter Axxent electronic brachytherapy source, to within 5% and 3mm of published values.

The specific aims for testing this hypothesis:

1. Write code specifically for use with PRESAGE dosimeters in MATLAB to extract data for TG-43U1 analysis.
2. Determine the TG-43U1 parameters of the Xofter Axxent electronic brachytherapy source using PRESAGE dosimeters. TG-43U1 parameters will be extracted from the optical scans of the irradiated dosimeters via the code developed in Specific Aim 1.
3. Compare PRESAGE-measured TG-43U1 parameters for the Xofter Axxent electronic brachytherapy system with published parameters.

2 Methods & Materials

2.1 Dosimeter Design

Two formulations of PRESAGE™ were irradiated with the Xofter source - a "soft" batch (#46), and a "hard" batch (#45). According to the manufacturer, the difference between the two formulations is the polyurethane used - soft versus hard. The soft batch is more tissue-equivalent, but will bleach over time (a new experimental formula), and the hard dosimeters are the usual PRESAGE formulation. The dosimeters are approximately 1 kg, 12 cm in height, and 11 cm in diameter. Due to the size of the DMOS tank and the field-of-view of the DMOS camera, the dosimeters cannot be much larger than this. The size of the dosimeters also limits the maximum radius to which the dose can be measured to approximately 5 cm.

Both formulations of PRESAGE were cast with two different channel sizes, as seen in Figures 8-9. The two channel sizes were first suggested by Olivia Huang's research using AgX100 I-125 seeds (7). She found that because PRESAGE reacts linearly to dose, a large dose near the source will cause a great change in OD, such that when the dosimeter is optically CT-scanned, imaging through the center becomes difficult since the dye is so dark there. However, if the dosimeter is irradiated with the source in a PRESAGE plug (seen in Figure 10) in a large channel, the plug may be removed when the dosimeter is optically CT-scanned, and the center of the dosimeter won't be as dark since the plug has been irradiated to the high dose instead of the dosimeter. In Huang's experiment, a higher

dose was given to the large channel dosimeters than to the small channel dosimeters so that the dose at large radii would be readable in the scanner. Likewise, a smaller dose was given to the small channel dosimeters so that the dose in the center of the dosimeter could be read by the scanner. This way, the dose throughout the dosimeter could be measured. However, Huang also found that a higher dose than she used could be given to the dosimeters, and it was decided that for this experiment, the same, higher dose would be given to both channel sizes and both PRESAGE formulations.

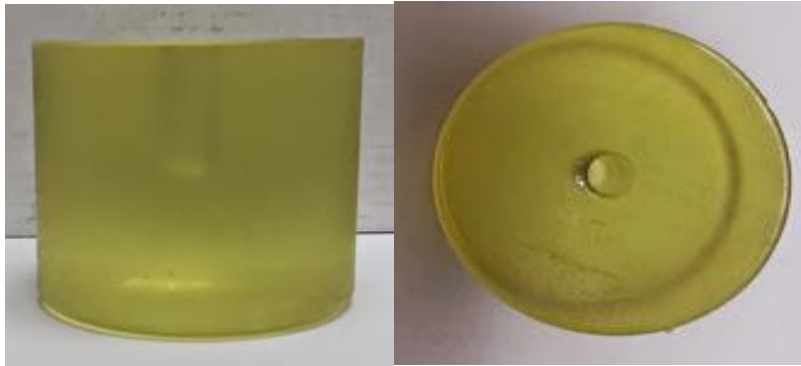


Figure 8. PRESAGE with 1.5 cm diameter large channel (soft batch).



Figure 9. PRESAGE with 5.3 mm small channel (hard batch).



Figure 10. Irradiated plug for large channel dosimeters; note the darkened end where the x-ray tube was located within the Xofig catheter within the plug.

For this experiment, the larger channel size was 1.5 cm in diameter, with a PRESAGE plug, or insert, that fit exactly into the channel to keep the Xofig source secure in

a homogenous attenuating medium. The plug was removed for imaging, and the channel was filled with matching fluid. The smaller channel size was 5.1 mm in diameter, sized so that the Xofter source fit perfectly in place. From Huang's thesis, the smaller channel size was used to measure doses out to a radius of 2.5 or 3 cm, and the larger channel size was used to measure doses out to the edge of the dosimeter, at a radius of approximately 5 cm. For this experiment, however, it was decided that both channel sizes and both formulations could be irradiated to 15 Gy at 1 cm without any OD read-out issues.

2.2 Treatment setup and delivery

2.2.1 Dose calibration

Five cuvettes containing the soft PRESAGE formulation and ten cuvettes containing the hard PRESAGE formulation were requested from the manufacturer along with the 1 kg dosimeters used for this experiment. Cuvettes, seen in Figure 11, are small plastic vials, approximately 1 cm square and approximately 5 cm long, containing PRESAGE. Cuvettes are used to determine absolute dose for different PRESAGE batches, since PRESAGE is a relative dosimeter.

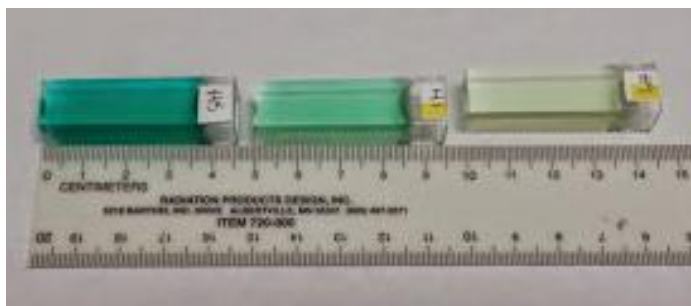


Figure 11. PRESAGE cuvettes for dose calibration.

Prior to irradiation, the cuvettes were labeled (S1-S5 and H1-H10) and their absorbance at 633 nm was determined in a Genesys 20 spectrophotometer (Thermo Scientific, Waltham, MA). This established a background optical density. The cuvettes were scanned in two directions to ensure the optical density was approximately the same throughout.

The cuvettes were irradiated with an orthovoltage machine at 125 kVp, which has a dose rate of 74.76 cGy/min. The cuvettes should have been irradiated at 75 kVp, the beam closest to the 50 kVp Xofter energy characterized and available at this institution. However, the cuvettes were inadvertently irradiated with the 125 kVp beam instead. The doses to the cuvettes were originally calculated assuming the 75 kVp beam, but when the error was realized, the doses were recalculated.

For the irradiation setup, the cuvettes were placed on top of approximately 10 cm of solid water to prevent backscatter, and within an acrylic sheet with a cutout in the center large enough to place four cuvettes side-by-side. Any gap within the acrylic sheet was filled with previously irradiated cuvettes for consistent material densities. This setup can be seen in Figure 12. The SSD was 50 cm, the field size was 10 cm by 10 cm, the irradiation was to the surface, and the dose was calculated to muscle.



Figure 12. Cuvette irradiation setup (7).

The cuvettes were given half their total dose on one side, then turned over 180° and irradiated to the rest of the dose. This was to ensure that the cuvettes were evenly irradiated to the total dose, so the dose profile would not have any steep gradients. The cuvettes were irradiated to an evenly-spaced range of doses, as seen on the x-axes in Figures 13-14, with one held aside so a “zero” dose mark could be obtained. The cuvettes were irradiated to different doses so a dose calibration curve could be obtained - OD versus dose.

After irradiation, the cuvettes were scanned in the same spectrophotometer at 633 nm, again in two directions, and the ODs recorded. A graph of OD versus dose was created for both batches of cuvettes, as seen in Figures 13-14. Net OD was calculated by subtracting the average of the pre-irradiation scan ODs from the average of the post-irradiation scan ODs.

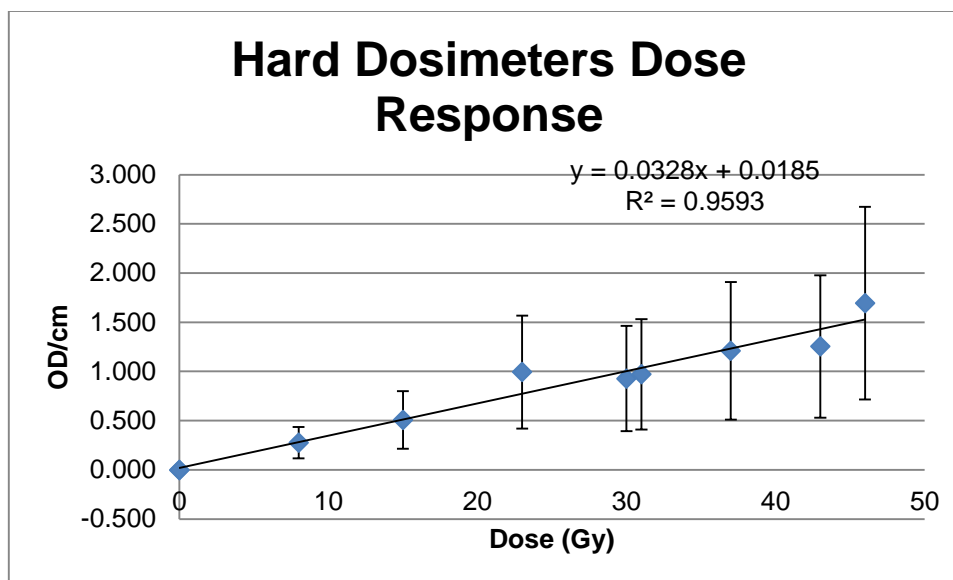


Figure 13. Hard dosimeters dose response curve with a linear fit and corresponding R^2 value.

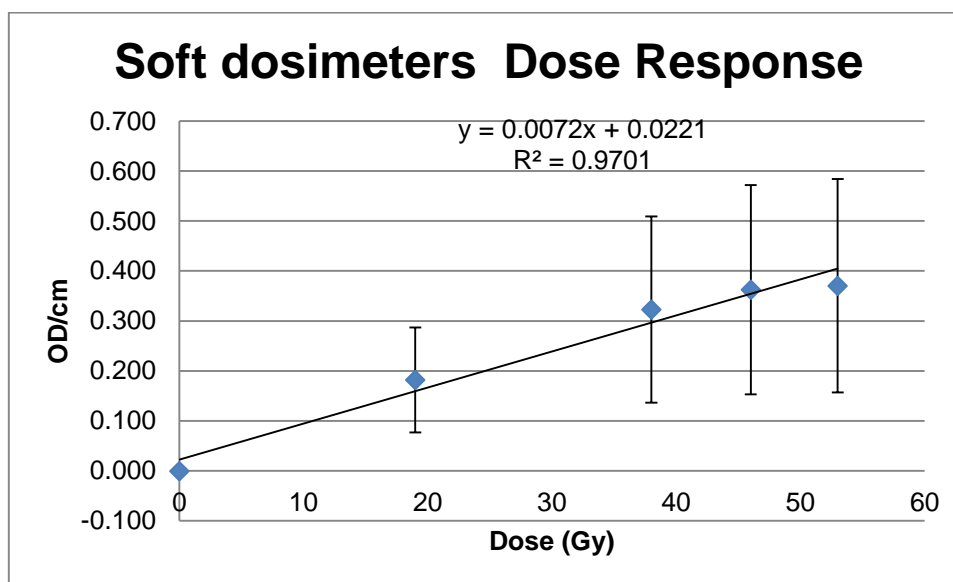


Figure 14. Soft dosimeters dose response curve with a linear fit and corresponding R^2 value.

2.2.2 Pre-irradiation

The dosimeters were stored in black bags in a refrigerator kept at 4° C; PRESAGE is light and heat sensitive, and this procedure reduces background exposure of the dosimeters. Prior to scanning or irradiation, the dosimeter was removed from the fridge and allowed to warm up to room temperature for at least six hours.

Eight total dosimeters were used in this experiment, four of the hard formulation, and four of the soft. Of the four hard dosimeters, one had a large channel, and three had a

small channel. Of the four soft dosimeters, two had a large channel, and two had a small channel. The dosimeters all had a small base glued on the bottom so they could be reproducibly placed and scanned in the DMOS. Since there were two different formulations, two different refractive index (RI) matching fluid compositions had to be created prior to the pre-irradiation scans. The soft dosimeters were scanned first; mineral oil was used to lower the RI to approximately 1.485. Next, the hard dosimeters were scanned; cinnamate was added to the tank to raise the RI to approximately 1.495.

Since UT MD Anderson does not have a Xofter source, after the dosimeters were pre-irradiation scanned to obtain a measurement baseline, they were shipped in a light-tight box to the UWADCL.

2.2.3 Treatment delivery

The Xofter Axxent controller is used to deliver treatment in the clinic. However, for this experiment, a Modulation Test Fixture (MTF), seen in Figure 15, provided by the manufacturer to the UWADCL was used. It mimics the electronic controller and TPS; it allows the user to adjust the tube voltage and current, among other settings. The MTF uses a Monte Carlo software package to create "treatment plans," which allow time for the source voltage and current to ramp up and ramp down. Well chamber measurements can be made in either the provided Standard Imaging shielded well chamber (identical to the one provided with the commercial unit) or the NIST-calibrated Standard Imaging well chamber; for this experiment, measurements were taken in the NIST-calibrated well chamber.



Figure 15. MTF at UWADCL.

Due to the complicated procedures required to run the MTF, the staff at UWADCL ran the unit according to the irradiation time calculation provided to them. The irradiation time calculations had the units minutes per unit air kerma (in U), so that when the well chamber measurement of the Xoft source was taken, irradiation time was solved for and then plugged into the Monte Carlo system. The manufacturer gave the air kerma strength of the selected source, provided by Xoft (Xoft, San Jose, CA), as 126095 U. The UWADCL calibrated air kerma strength for this source was 1.180×10^{12} U/A.

Initially, the calculated treatment time was less than one minute, which would introduce large ramp up errors into the dose calculations. To lengthen the treatment time, the weaker of the two provided Xoft Axxent sources was selected for use (S_K stated previously); unfortunately, this only added a few seconds to the total irradiation time. To further lengthen the treatment time, the treatment amperage was lowered; test protocols were run at both 200 μ A and 100 μ A. At 100 μ A, the treatment time was three minutes, and so the ramp error was greatly reduced. Previous (currently unpublished) studies at UW have shown that operating the source at these lower currents is an acceptable method to lengthen treatment times to minimize ramping errors.

A protocol was created to run at 50 kV and 100 μ A for 180 seconds. This procedure was followed for all 8 irradiations. However, during all of the soft batch PRESAGE irradiations, the source arced part of the way into the irradiation. A new protocol was created for each of these cases to irradiate for the remainder of the 180 seconds. This introduced more ramp up error into the irradiation, but it did not change the total dose delivered by more than 2.7%.

For the irradiations, the dosimeters were placed in a cylindrical phantom, approximately 29 cm in diameter. Foam was used to reduce the diameter to approximately 21 cm, then the dosimeter was placed on a base that raised it approximately 5 cm above the bottom of the phantom. Rice was then poured around the dosimeter, which was still enclosed in a black bag to protect it from light. The rice, a tissue equivalent material, was used to produce backscatter that would be comparable to the backscatter of the ion chamber measurements and the Monte Carlo calculations. Rice was used instead of water because PRESAGE, particularly soft batch PRESAGE, is partially soluble in water. The dosimeter was centered in the phantom so that it was surrounded on all sides by approximately 5 cm of rice. For ease of transfer between dosimeters, a plastic bag was placed into the tank for the rice to be poured into and out of. This setup is shown in Figure 16.



Figure 16. Dosimeter shielded from light and surrounded by rice in phantom.

With the room lights out, the Xofter catheter was placed, either directly into the small channel or into the PRESAGE plug then into the large channel (seen in Figure 17). In either case, the catheter and plug were inserted to the very bottom of the channel. As stated previously, all dosimeters were irradiated to 15 Gy at 1 cm with a treatment time of 180 seconds. In the cases when the source arced, the 180 second treatment time was completed, but the dose was calculated to be closer to 15.41 Gy, due to the additional ramp up error. The dosimeters were shipped back to IROC-Houston post-irradiation, and scanned in the DMOS as soon as the experimenter returned.

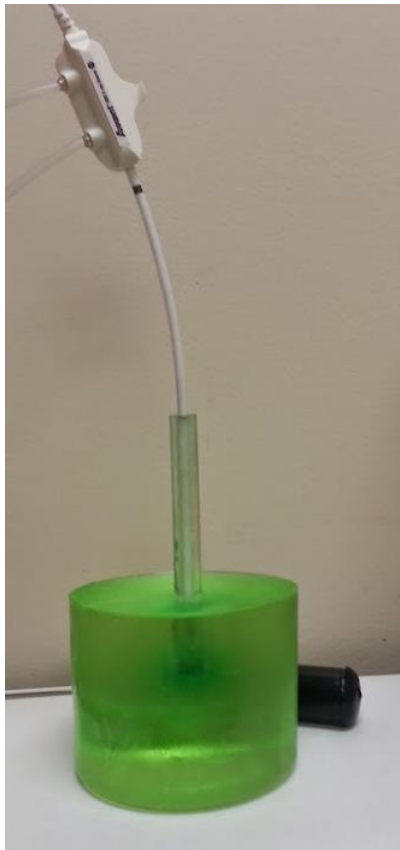


Figure 17. Xofter Axxent source inside plug inside PRESAGE dosimeter.

2.3 Imaging and analysis

2.3.1 Optical-CT imaging

The dosimeters were scanned post-irradiation according to the methods outlined in Chapter 1. Due to the two different PRESAGE batch formulations, the RI of the matching fluid was monitored and adjusted as needed to match the RIs used during the pre-irradiation scans. Reconstruction of the images was also performed according to the methods described in Chapter 1.

2.3.2 Data Acquisition in MATLAB

In an earlier work, to extract the TG-43U1 data from the DMOS optical-CT scans, the scans were imported into the Computational Environment for Radiotherapy Research (CERR) and the OD was scaled according to the calibration curve obtained from the cuvettes. Line profiles were taken, which create a plot of dose versus dosimeter radius, and parameters were input into an Excel spreadsheet for analysis. Since this is a lengthy process, only 12 points from each radius were taken and averaged together (7). To make data extraction faster and simpler, as well as to obtain more points for use in the average dose, code was written to do this instead.

Two separate scripts were written - one to calculate the radial dose function, called `radialunicorns.m`, and the other to calculate the anisotropy function, called `anisotropyunicorns.m`. The codes work in similar ways: they both take an average of the value of the data cube within an annulus. The coordinate system used to define the annulus in PRESAGE is depicted in Figure 18. The annulus is defined as 3 z-planes thick, centered around the anode's z-plane, with the inner and outer radii ± 0.5 mm from the defined radius given by Rivard et al. (1); an example annulus is shown in Figure 19. For the anisotropy function, averages were also taken every 10° for each given radius. The polar angles noted were also taken from Rivard et al. (1), for ease of comparison. The entire cube is searched for points within the annulus.

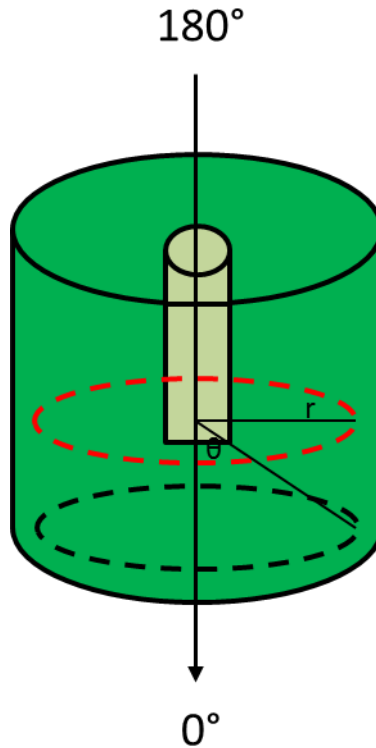


Figure 18. Diagram of the transverse plane (red dashed circle) and another measurement plane at θ (black dashed circle), in the PRESAGE dosimeter.

The average value of the data cube is output as an unnormalized average dose rate at that radius, or at that radius and angle.

These two codes are written out in Appendix B. To use them, the user must type the location of the input data cube file in the *.m file so it can be loaded, then run the script. This data cube is saved from the Reconstruction GUI discussed previously. The script will ask the user for the (x,y,z) center of the data cube, i.e., the location of the Xofter Axxent anode, from which point the script will do radius and angle calculations. The z-axis is defined in the data cube by the DMOS Reconstruction software, and MATLAB uses this definition when it imports the data cube. The x- and y-axes are less important because the radius and polar angle calculations are both performed with respect to the z-axis only. The user will also be asked to enter the size of the data cube (x,y,z). Both of these coordinate sets can be obtained by running GUIPhoenixFire.m, a code developed by a fellow lab group member, Slade Klawikowski, to extract dose from CyberKnife PRESAGE irradiations. A screenshot of the GUIPhoenixFire.m program is shown in Figure 20.

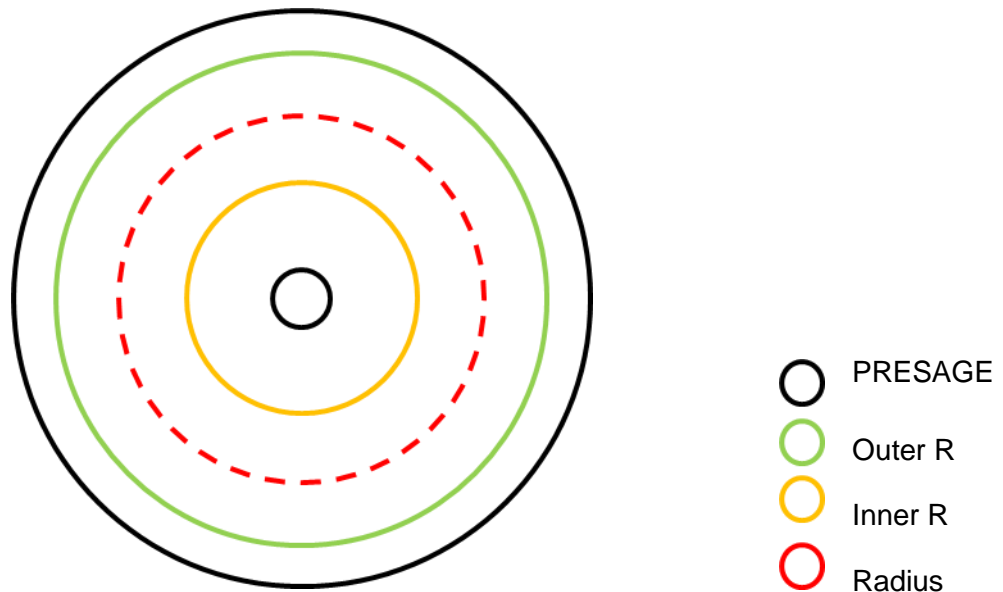


Figure 19. The image on the left is a top view of the dosimeter showing the annulus described; the z-axis points into the page. The dashed red line is the radius from which the delta is applied. The black circle at the center is the channel, and the black outline is the outer edge of the dosimeter.

Notice the sliders at the bottom of the GUI; the long slider allows the user to page through the optical-CT slices in z, and the x and y sliders that allow the user to select the center of the dosimeter. From these three sliders, the user can determine both the (x,y,z) center and the (x,y,z) extent of the data cube. The center of the dosimeter is not its measured center, but rather the point in the channel where the anode of the Xoft catheter is expected to be. When stepping through the z slices of the dosimeter in the PhoenixFire GUI, the anode was assumed to be in the last slice of the channel, as shown in Figure 20.

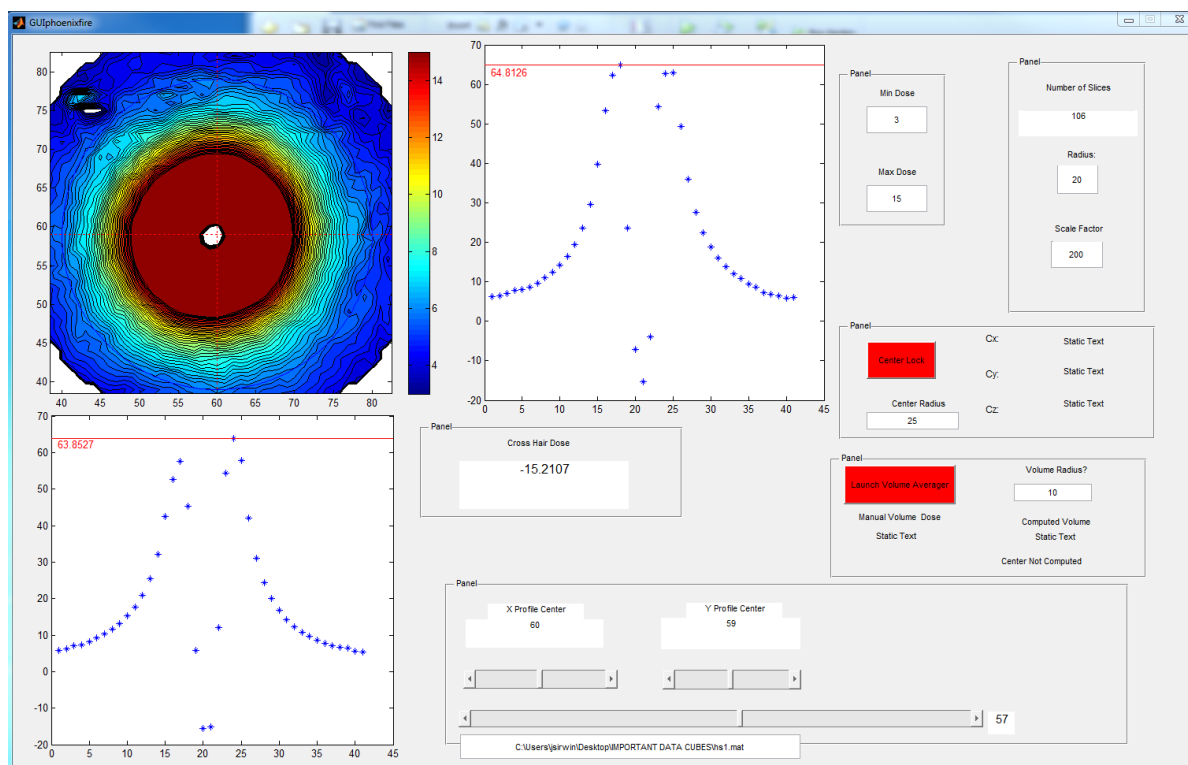


Figure 20. Screenshot of PhoenixFire GUI, showing z slice where anode is located.

The radialunicorns.m code output a MS Excel spreadsheet of the average relative dose rate within each annulus for each radius. The anisotropyunicorns.m code output a MS Excel spreadsheet also which contains the average relative dose rate for each radius and angle pair. The code allows the user to name select where to save the Excel files. The data within these files is used to calculate the TG-43U1 parameters, which are then compared to the TG-43U1 parameters given in Rivard et al. (1) for Specific Aim 3.

2.3.2.1 Testing the code

To ensure the scripts written worked correctly, a number of test scenarios were created where the outcome of the script could be estimated easily by the user. The first test was sending a data cube matrix of all ones through the script. The output of the script calculated the average value for each radius annulus as one, as expected. Next, a small (9x9x9) data cube matrix was created where the value of the data cube was equal to the radius at that point, e.g., at $r=3$, the value is 3. This test matrix returned expected results, i.e., the average value at $r=3$ was ~ 3 . As a final test, a data cube of similar size to those used in this project was run through the complete code. The data cube was taken from a CyberKnife irradiation, and had two peaks, one sharp and towards the top of the dosimeter, and one broad and flat, towards the bottom. The dose from these irradiations had some

angular dependence. The code was run twice, using both peaks as the center calculation point. The output results were as expected.

2.4 TG-43U1 Formalism

The AAPM TG-43U1 report is recommended for dosimetry analysis of a brachytherapy source. Until the AAPM Task Group No. 182 Report Recommendations on Electronic Brachytherapy Quality Management is released, TG-43U1 will be used.

Figure 21 shows the polar coordinate system as defined in the report and used here. The orientation of the Xofig source in this image is down the z-axis; the L bracket denotes the anode location. The report defines the point of interest as $P(r, \theta)$, and the reference point as $P(r_0, \theta_0)$, where r_0 is 1 cm and θ_0 is 90° or $\pi/2$ radians. These coordinates and points are used to determine the radial dose function and the anisotropy function.

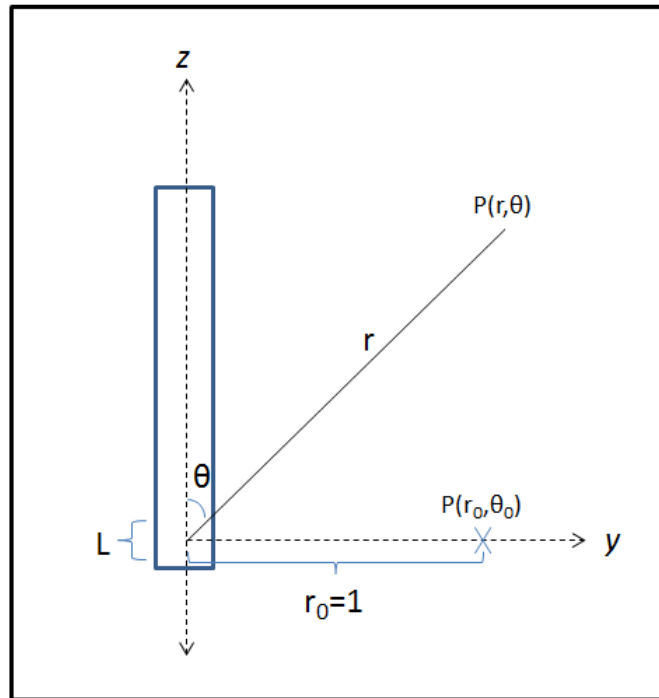


Figure 21. Modified TG-43U1 coordinate system for brachytherapy dose calculations. L is the active length of the source in centimeters, r is the distance from the center of the source to the point of interest $P(r, \theta)$ in centimeters, and θ is the polar angle between the radius r and the longitudinal (z) axis of the source. (17)

2.4.1 Air kerma strength.

Air kerma strength S_K is given in units of U, where $1 \text{ U} = 1 \text{ cGy cm}^2/\text{h} = 1 \text{ μGy m}^2/\text{h}$. TG-43U1 defines S_K as the air kerma rate in a vacuum due to photons of energy greater than δ , at a distance d, multiplied by the distance squared.

$$S_K = K_\delta(d)d^2 \quad \text{Eqn. 4}$$

The distance d is defined as the distance from the source center to the point of interest where S_K is specified. The energy cutoff δ is usually set to 5 keV to exclude low energy photons in the XOFT source emission spectrum that do not deliver significant dose past 0.1 cm in tissue. The air kerma rate is generally measured with a free air device at large (~1m) distances.

Air kerma strength values are reported by the manufacturer, but can also be calibrated by an ADCL, which is traceable to the 1999 NIST standard for I-125 model MED3631-A/M (17). However, for the Xofter source, there is no NIST standard for air kerma strength, so the workaround calibration procedure is used.

2.4.2 Air kerma rate calibration

Because there is no NIST standard for this source, a workaround has been created by the UWADCL by combining the procedures in TG-43U1, the task group on brachytherapy dosimetry, and TG-61, which covers low energy (40-300 kV) x-ray beam dosimetry.

First, the air kerma of an I-125 seed is measured in the shielded well chamber which comes with the Xofter system, using the insert that places the seed at the “sweet spot.” The sweet spot is defined as the point in the well chamber at which the reading from the source is at a maximum.(14) The calibration coefficient “C” is calculated as the air kerma divided by the corrected chamber current. Next, the Xofter source is placed in an Attix free air chamber (FAC) and the output is measured. The ratio “R” is taken of the Xofter and I-125 coefficients, so that $N_{SK} = R \times C$, and N_{SK} is defined as the Xofter air kerma in the well chamber. This N_{SK} value is placed in the TPS as the nominal air kerma, and is compared to each new source's measured air kerma in the well chamber.

In clinical use, the air kerma strength of the source is measured prior to each fraction in the attached shielded Standard Imaging well chamber, using the insert described previously. This air kerma strength measurement, in U, is input into the TPS, which calculates dwell time and position.

The attached well chamber is calibrated every two years by the ADCL, as per requirements. The Xofter manual speaks of compensated air kerma, which is defined as air kerma that is temperature and pressure corrected. The final equation for compensated air kerma is, in units of U:

$$S_K = N_{SK} \times P_{elec} \times M_{raw} \times C_{T,P} \times P_{altitude} \quad \text{Eqn. 5}$$

2.4.3 Dose rate

The 2D dose rate to water equation as specified in TG-43U1 is

$$\dot{D}(r, \theta) = S_K \times \Lambda \times \frac{G_L(r, \theta)}{G_L(r_0, \theta_0)} \times g_L(r) \times F(r, \theta) \quad \text{Eqn. 6}$$

However, for this experiment, $G_p(r, \theta)$ and $g_p(r)$ are used, as was done in the Rivard et al. paper (1). This formalism assumes that the source has a cylindrically symmetric dose distribution with respect to the z-axis, and that the radiation emanates from a point source. Dose rate is in units of cGy per hour. The dose rate in PRESAGE was calculated using this equation and the tables in the Xofter manual (24). These tables are located in Appendix A. All dosimeters were irradiated to the same dose, so all dosimeters have the same calculated dose rate. The calculated dose rate for the PRESAGE irradiations was

$$\dot{D}(1 \text{ cm}, 90^\circ) = 126095 \text{ U} \times 0.709 \text{ cGy h}^{-1} \text{ U}^{-1} \times 1 \times 1 \times 1 = 894 \text{ Gy h}^{-1} \quad \text{Eqn.7}$$

2.4.4 Dose rate constant

TG-43U1 defines the dose rate constant in water (Λ) as the ratio of the dose rate at the reference point to the air kerma strength.

$$\Lambda = \frac{\dot{D}(r_0, \theta_0)}{S_K} \quad \text{Eqn. 8}$$

Λ has units of cGy per hour per U. The dose rate constant for Xofter was measured in both solid and liquid water, as well as calculated using a Monte Carlo model. The unfiltered source dose rate constant was not published in Rivard et al. (1), and so is taken from the Xofter Operator's Manual.

	Dose Rate Constant (cGy hr ⁻¹ U ⁻¹)
Unfiltered 50 kV source	0.709

Table 3. Dose rate constant (24)

2.4.5 Geometry function

According to TG-43U1, the geometry function provides an inverse square law correction based on the approximate spatial distribution of radioactivity in the source. Therefore, there is both a point source and a line source approximation. The effective length L_{eff} of the anode in the Xofter source is 0.1 cm. Rivard et al. (1) states that at this small L_{eff} , the difference between using the line source approximation and the point source approximation is not more than 1%, therefore they set $L_{\text{eff}} = 0$, and use the point source approximation for the geometry function. As this paper is comparing its results to that paper, the same steps will be taken here. Therefore, the geometry function $G_p(r, \theta)$ is $1/r^2$ or $(r_0/r)^2$, where r and r_0 are defined as before.

Radius (cm)	1	2	3	4	5
$G_p(r)$	1	4	9	16	25

Table 4. Geometry factors for a point source.

2.4.6 Anisotropy function

TG-43U1 defines the 2D anisotropy function $F(r, \theta)$ as the variation in dose as a function of polar angle relative to the transverse plane (i.e., at $\theta=90^\circ$). The equation is

$$F(r, \theta) = \frac{\dot{D}(r, \theta) G_L(r, \theta_0)}{\dot{D}(r, \theta_0) G_L(r, \theta)} \quad \text{Eqn. 9}$$

$F(r_0, \theta_0) = 1$, and will decrease as r decreases, as θ approaches 0° or 180° , as encapsulation thickness increases, or as photon energy decreases. For this experiment, to match the Rivard et al. data (1), the point source geometry function $G_p(r, \theta)$ was used. The values for the anisotropy function for Xofig are shown in the table below, taken from the Rivard et al. paper. (1, 24)

$\theta(\text{degrees})$	$F(2, \theta)$	$F(3, \theta)$	$F(5, \theta)$
0	0.993	1.018	1.050
10	1.001	1.027	1.054
20	1.013	1.037	1.059
30	1.024	1.042	1.065
40	1.052	1.065	1.075
50	1.072	1.080	1.080
60	1.075	1.079	1.075
70	1.063	1.065	1.062
80	1.037	1.038	1.036
90	1.000	1.000	1.000
100	0.953	0.954	0.950
110	0.895	0.896	0.894
120	0.820	0.824	0.825
130	0.709	0.721	0.731
140	0.564	0.590	0.616
150		0.426	0.473
160			0.364

Table 5. Measured anisotropy function at 50 kV (1)

The anisotropy function in PRESAGE was calculated using the above equation, which reduces to

$$F(r, \theta) = \frac{\dot{D}(r, \theta)}{\dot{D}(r, 90^\circ)} \quad \text{Eqn. 10}$$

The dose rate values were pulled from the data using the script, as described in the Data Acquisition section. The dose rate values were corrected for zero dose as described in Chapter 3.

2.4.7 Radial Dose Function

The radial dose function $g_p(r)$ accounts for dose falloff due to attenuation and scattering; this does not include dose falloff from the inverse square law, since that is already accounted for in the geometry function. The equation for a point source (1D) is

$$g_p(r) = \frac{\dot{D}(r, \theta_0) G_p(r_0, \theta_0)}{\dot{D}(r_0, \theta_0) G_p(r, \theta_0)} \quad \text{Eqn. 11}$$

Below are the values from Rivard et al. (1).

r (cm)	$g_p(r)$
1.0	1.000
1.2	0.920
1.4	0.848
1.6	0.786
1.8	0.732
2.0	0.683
3.0	0.511
4.0	0.399
5.0	0.317

Table 6. Radial dose function values measured at 50 kV (1)

The radial dose function in PRESAGE is calculated using the equation above, which reduces to

$$g_p(r) = \frac{\dot{D}(r, 90^\circ) \times r^2}{\dot{D}(1, 90^\circ)} \quad \text{Eqn. 12}$$

The dose rate values were pulled from the data using the script, as described in the Data Acquisition section. The dose rate values were corrected for zero dose as described in

Chapter 3. Note that for the radial dose function, the measurements are taken at different radii, but all in the transverse ($\theta = 90^\circ$) plane.

3 Results for Xofter Source

3.1 Soft Dosimeter Batch

The soft PRESAGETM dosimeters were excluded from the results. The formulation was created so it would fade over time after irradiation, and it was observed that in the short time between irradiation with Xofter at the UWADCL and the post-irradiation scan at IROC-Houston, the signal in the soft dosimeters faded too much to provide useful dose information. Figure 22 shows the pre-irradiation and post-irradiation images for comparison. It is also noted here that the Xofter source formed an electric arc during each irradiation of a soft dosimeter, but not during any of the hard dosimeter irradiations. This was thought to be a random effect, the only result of which was the soft dosimeter irradiations were then forced to be delivered in a fractionated manner, e.g., one 120 second irradiation followed by a 60 second irradiation, instead of one 180 second irradiation.

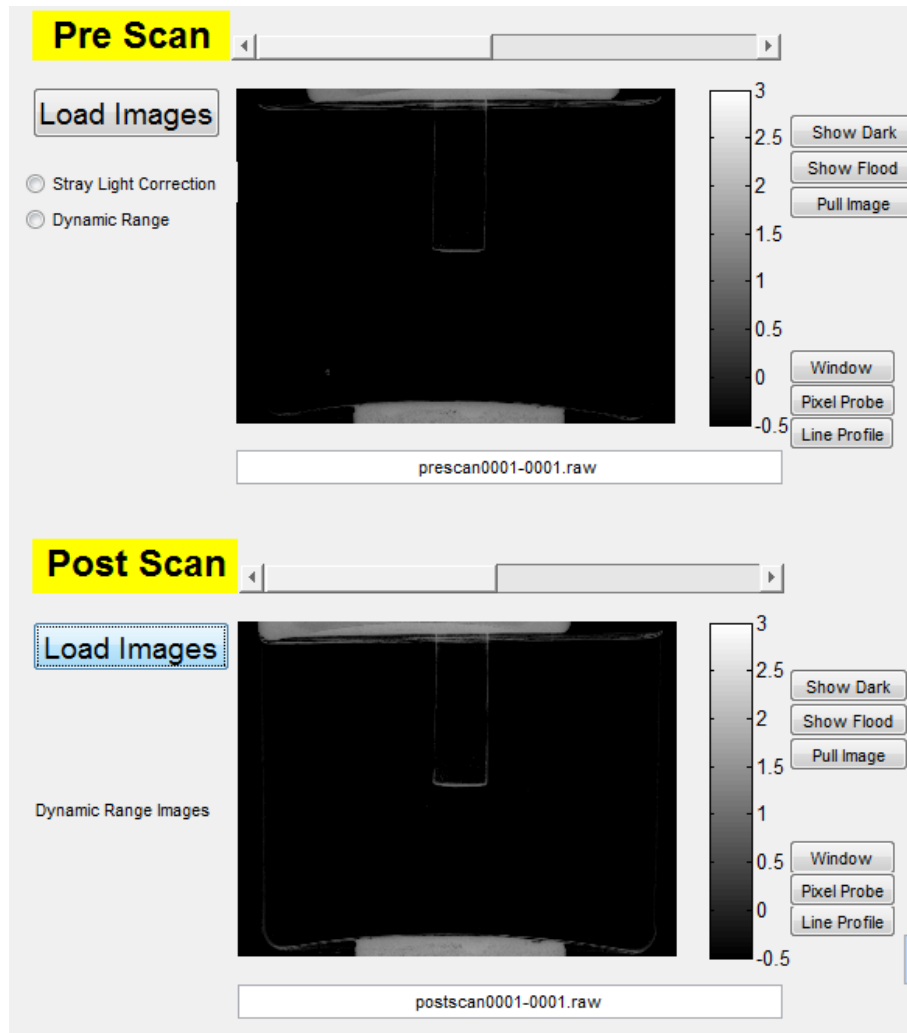


Figure 22. Prescan and postscan images of a soft dosimeter with a large channel. Note that the irradiation seems to have had almost no effect on the dosimeter, probably due to fading.

3.2 Radial dose function

The radial dose function measured and calculated in PRESAGE is shown in Table 7. This data is taken from a single small channel dosimeter; the average radial dose function data from all four dosimeters is shown in Appendix C. PRESAGE measurements at 4 cm radius were removed from the analysis due to the negligible level of signal above the background that existed there; no data was expected at $r = 5$ cm due to the size of the dosimeters and edge effects. The PRESAGE-measured radial dose functions for $r = 1$ cm to $r = 2$ cm agree with those calculated by and Rivard et al. (1) to within 6%. However, at $r = 3$ cm, the radial dose function measured in PRESAGE shows an under-response by 51.1%; this suggests that the noise level at $r = 3$ cm is comparable to the measurable dose at that radius, probably due to the age of the dosimeter during its final scan and the exacerbation

of edge effects in PRESAGE as the dosimeter ages. A graphical representation of the radial dose function comparison is shown in Figure 23.

r (cm)	Rivard et al. value	PRESAGE value	Percent Error
1	1	1	0
1.2	0.920	0.958	4.2
1.4	0.848	0.894	5.5
1.6	0.786	0.831	5.7
1.8	0.732	0.751	2.6
2	0.683	0.689	0.9
3	0.511	0.250	51.1

Table 7. Radial Dose Function Comparison

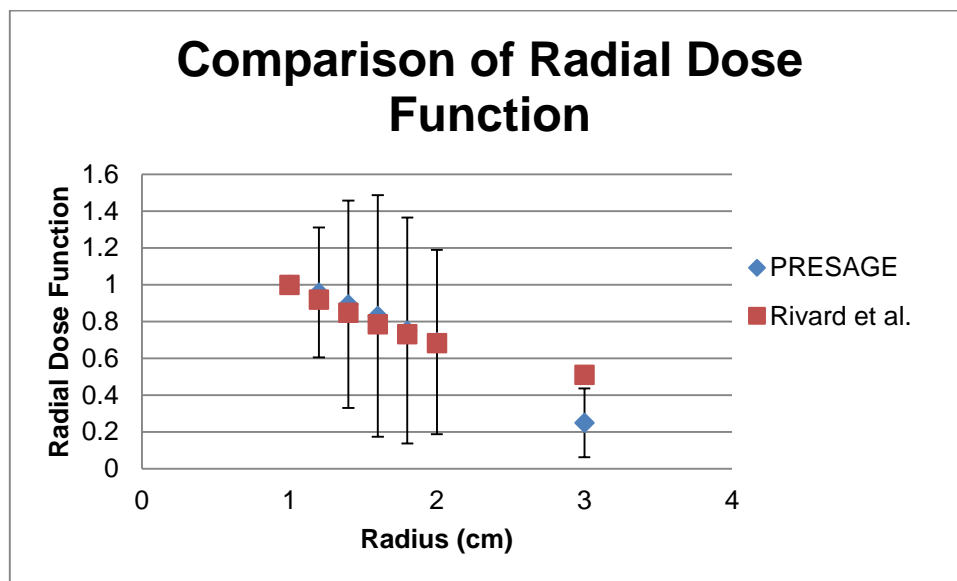


Figure 23. Graphical comparison of the radial dose function. Rivard et al. is in blue diamonds, and PRESAGE is in red squares.

3.3 Anisotropy function

Table 8 shows the anisotropy function measured and calculated in PRESAGE. Refer to Table 5 for the Rivard et al. anisotropy function values. The data from PRESAGE at $r = 5$ cm was not included because no data is expected at that radius, due to the size of the dosimeter and edge effects of PRESAGE. The angles 140° and 160° are very close to

the channel, subjecting the readings there to edge effects. Table 9 shows the percent error values for the anisotropy function, comparing the Rivard et al. (1) values to the PRESAGE values.

$\theta^\circ/r(\text{cm})$	2	3
0	1.260	1.371
10	1.202	1.239
20	1.193	1.315
30	1.280	1.264
40	1.307	1.266
50	1.285	1.299
60	1.346	1.261
70	1.316	1.224
80	1.196	1.137
90	1.000	1.000
100	0.864	0.930
110	0.693	0.835
120	0.641	0.708
130	0.832	0.631
140	1.316	0.542
150	1.029	2.154
160	1.231	4.970

Table 8. Anisotropy function measured in PRESAGE

Ignoring the extreme outlier for each radius ($\theta=140^\circ$ for $r=2$, and $\theta=150^\circ$ for $r=3$), the $r = 2$ cm values are within 27% of the Rivard et al. data, and the $r = 3$ cm values are within 35% of the Rivard et al. data.

$\theta^\circ/r(\text{cm})$	2	3
0	26.9	34.6
10	20.1	20.6
20	17.8	26.8
30	25.0	21.3

40	24.3	18.9
50	19.9	20.3
60	25.2	16.8
70	23.8	14.9
80	15.4	9.5
90	0.0	0.0
100	9.3	2.5
110	22.6	6.8
120	21.9	14.1
130	17.3	12.5
140	133.3	8.2
150		405.6
160		

Table 9. Anisotropy function: Percent Error

Table 10 shows the standard deviation and Table 11 shows the coefficient of variance expressed as a percent for the PRESAGE anisotropy function data. These values are lower closer to $\theta = 90^\circ$, and increase as θ moves away from the transverse plane. This suggests that the measurements taken closest to the source are the most accurate; measurements in PRESAGE of the dose distribution from the Xofig appear to have a more rapid falloff than expected at large radii and at polar angles further from the transverse plane.

$\theta/r(\text{cm})$	2	3
0	0.589	0.375
10	0.557	0.349
20	0.516	0.342
30	0.514	0.322
40	0.445	0.271
50	0.360	0.223
60	0.358	0.127
70	0.345	0.060
80	0.162	0.038

90	0.000	0.000
100	0.090	0.046
110	0.153	0.115
120	0.127	0.079
130	0.339	0.166
140	1.361	0.238
150	1.043	2.025
160	1.112	7.074

Table 10. PRESAGE Anisotropy function: Standard Deviation

$\theta^\circ/r(\text{cm})$	2	3
0	46.8	27.4
10	46.3	28.1
20	43.2	26.0
30	40.2	25.5
40	34.0	21.4
50	28.0	17.2
60	26.6	10.1
70	26.2	4.9
80	13.5	3.3
90	0.0	0.0
100	10.4	4.9
110	22.1	13.8
120	19.9	11.2
130	40.7	26.3
140	103.4	43.9
150	101.3	94.0
160	90.4	142.3

Table 11. PRESAGE Anisotropy Function: Percent Coefficient of Variance

Figures 24 and 25 plot the anisotropy function at both radii and compare the Rivard et al. values with the PRESAGE values.

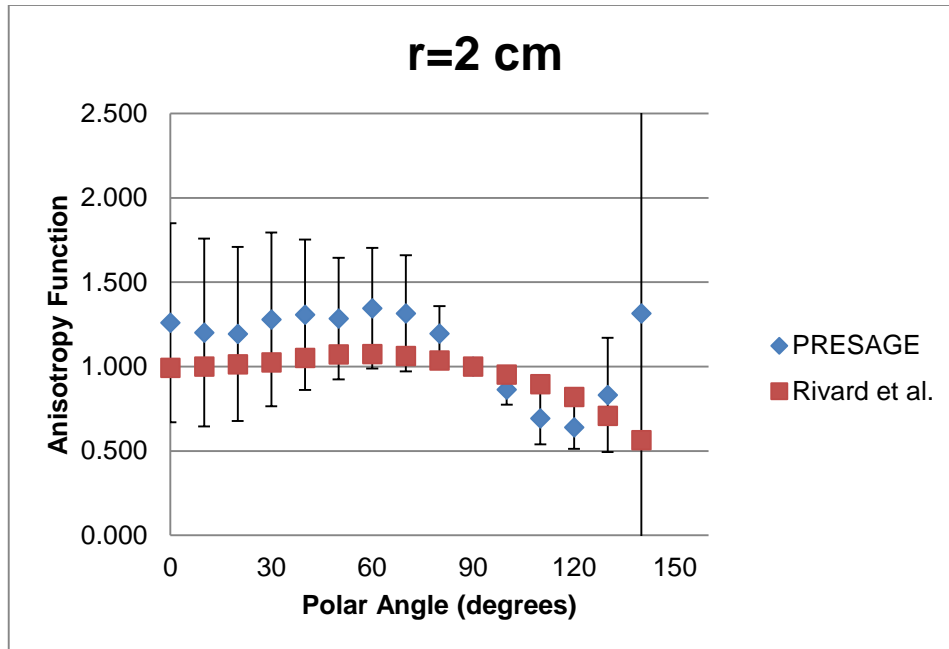


Figure 24. Anisotropy function for r=2cm.

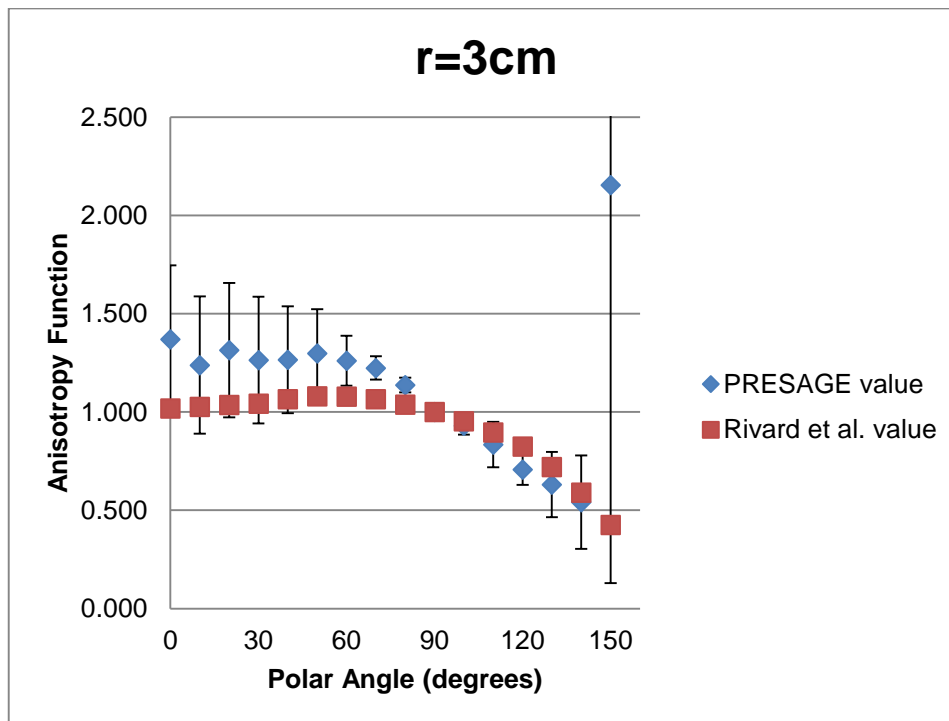


Figure 25. Anisotropy function for r=3cm.

4 Discussion

4.1 Concentric Rings Artifact

During the initial data analysis process, concentric rings were seen in the final data images; an example of this artifact is shown in Figure 26. These artifacts varied in thickness, brightness, and location, but were centered in the dosimeter and not around the channel, as might have been expected. These artifacts made the data past a radius of ~3 cm in the dosimeters unusable. An investigation was undertaken to determine the artifacts' cause and possible solutions.

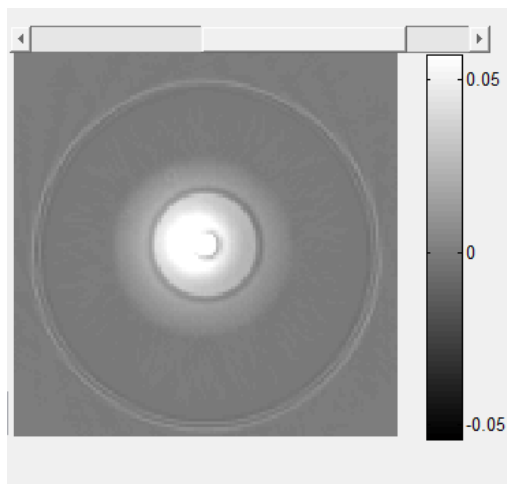


Figure 26. Reconstructed image showing the concentric ring artifact which is centered in the dosimeter and not around the dosimeter's channel.

The floods and dark images were checked to determine if there were any streaks that could be causing the rings. Different center of rotation (COR) columns were used in the image reconstructions as an inappropriate COR can cause the appearance of rings. A stray light correction was performed. Different floods were taken and used to reconstruct the images again. Pre-irradiation and post-irradiation scans were reconstructed separately and inspected. The rings appeared in both sets of images, though the appearance of the rings differed in each image; an example of these results is shown in Figure 27. The post-irradiation scan was repeated and reconstructed for each dosimeter, but the rings remained. Two unirradiated dosimeters were scanned, one from each batch, then reconstructed as pre-irradiation scans only. The artifacts were visible in those images as well. No other lab group members had seen these concentric rings in any current or previous data, and no one had used the same PRESAGE™ batches as were used here. A literature search was done, but the only concentric ring artifacts found were in gel dosimeters, and the causes of which did not apply to PRESAGE dosimetry (47, 48).

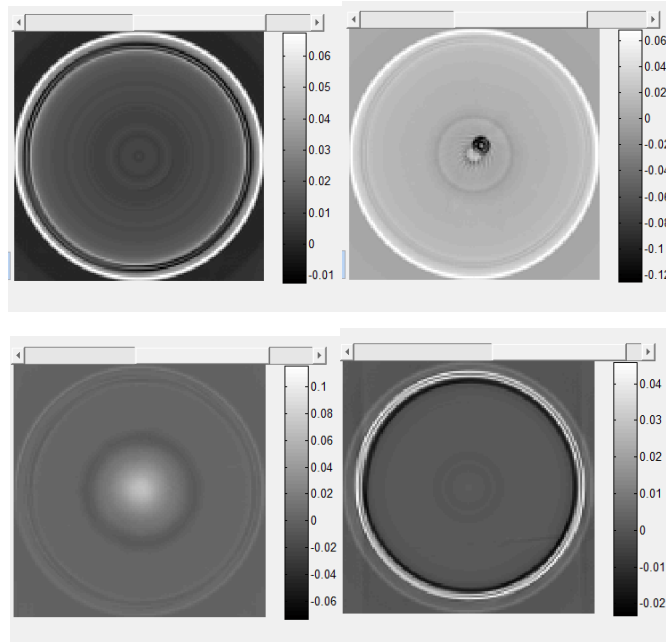


Figure 27. Top row shows pre-irradiation scans of two different dosimeters. Bottom row shows post-irradiation scans of two other dosimeters. Note the differing appearance of the rings in each image.

Finally, a query was sent to Titania Juang at Duke University. By looking at the number of counts per pixel in the RAW images, she determined that the flood and the projection images had been taken at different shutter values. The projection images were taken at a much higher shutter value than the flood, so that when the flood was used to correct the projection images during reconstruction, negative counts resulted in the final image. The flood image was darker than the dosimeter in the projection image, and had counts that were ~ 1000 lower than the projection images' counts; this can be seen in Figure 28.

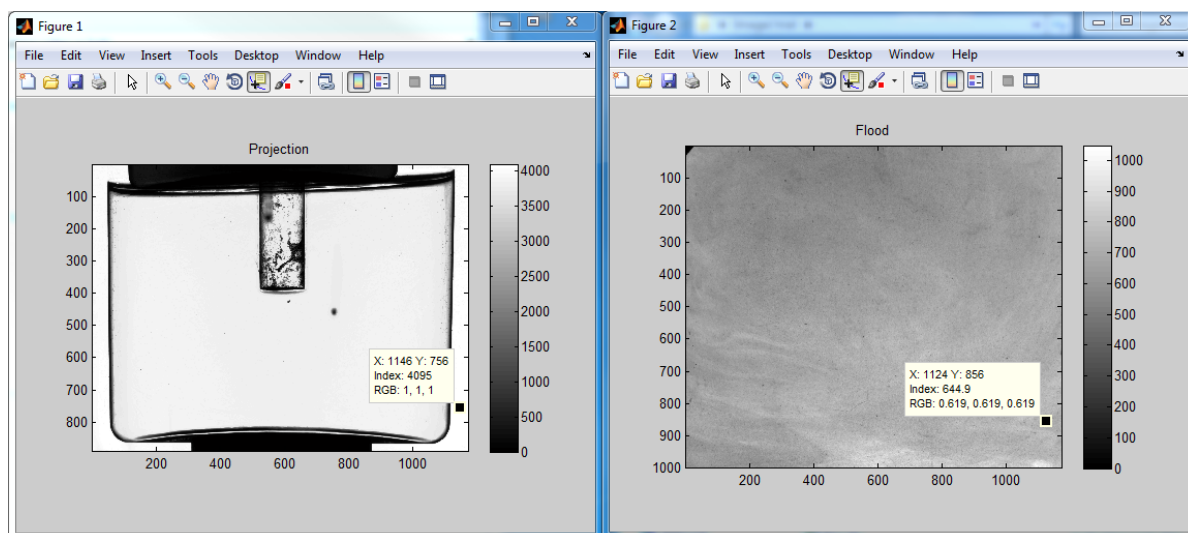


Figure 28. Projection image on left with Index (counts) of 4095. Flood image on right with Index at same location as in projection image of 644.9, giving a delta of over 3000.

This count difference was confirmed. Since the issue was with the projection images, which could not be retaken due to time constraints, the RAW projection images were pulled into MATLAB. MATLAB's image processing tools were explored as a possible solution. A post-irradiation projection image was darkened using the 'brighten(-0.5)' command. The new image, seen in Figure 29, showed that there was no data outside a radius of approximately 3 cm because the dosimeter there had been washed out by so much light due to the high shutter value. The same was done to a pre-irradiation projection image with the same result. In these darkened images, the cause of the concentric rings could be seen. It is theorized that the cause of the rings is the non-homogeneous light field of the IROC-Houston DMOS. It was already known that the field was darker in the center and brighter at the edges, but now images of how the light field brightness changes with radius show this inhomogeneity in more detail. This phenomenon had not been seen until now because other lab members used the correct shutter setting and did not use such large dosimeters as were used here. Since image processing could not improve the amount of data available in the images, another solution was attempted.

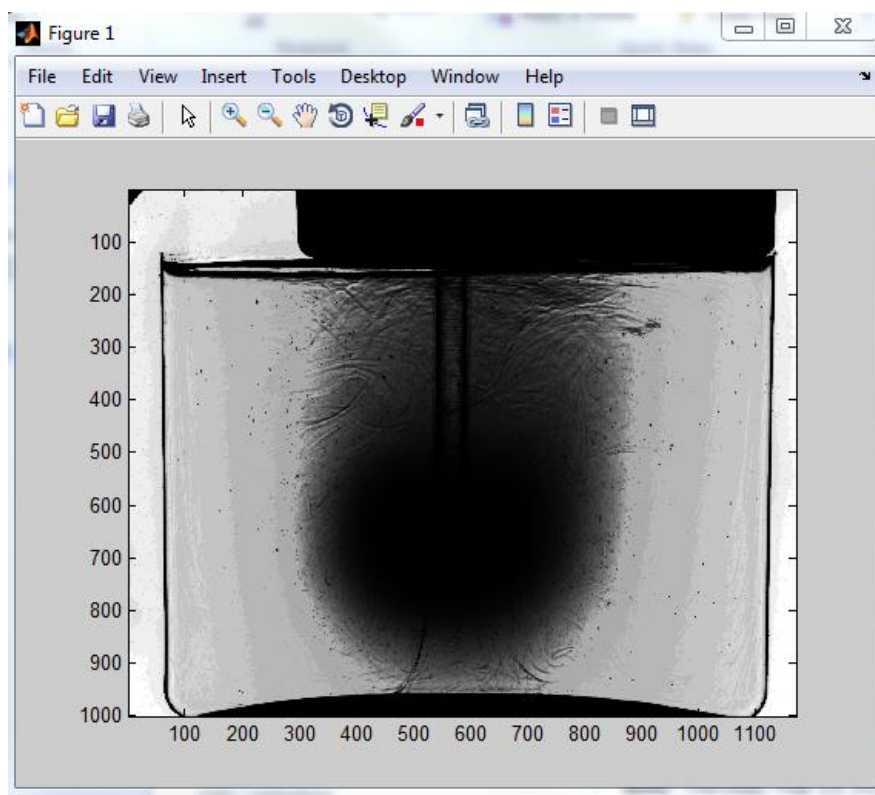


Figure 29. The extent of the available data (300-900 on the x-scale) can be seen in this darkened image of a post-irradiation scan projection image. Also seen are the causes of the concentric rings in the reconstruction images (bands of different contrast at 200, 300, 800, and 900 on the x-scale).

4.2 Solution to Remove the Artifact

The post-irradiation scans for the hard dosimeters were retaken with the correct shutter setting; an example projection image is shown in Figure 30, and compared to a flood image taken at the same shutter value. In Figure 31 is an image showing the absence of artifacts in the retaken image. The shutter setting was not discussed in the RPC DMOS Scanning Guide (39) and had been left out of lab member training. This issue has now been remedied. The scans were reconstructed as post-irradiation scans only, since the pre-irradiation scans could not be retaken. The data analysis was performed using these reconstructed post-irradiation scans. However, since these post-irradiation scans were performed 2 months after the irradiation, the dosimeters have aged. Older dosimeters are darker overall, and the radiation signal faded. Furthermore, edge effects are exacerbated in older dosimeters. The data obtained from the new post-irradiation scans will be subject to these age effects, and will not compare well with the Rivard et al. (1) data.

However, since the “post scan” only reconstruction was performed, no subtraction of background OD value in the dosimeter was completed. To remedy this, the dose rates at

large radii for each dosimeter were plotted and a background value was chosen at the point where the data appeared to level out in the plot. This background value was then subtracted from all dose rates. An example of this plot is shown in Figure 32.

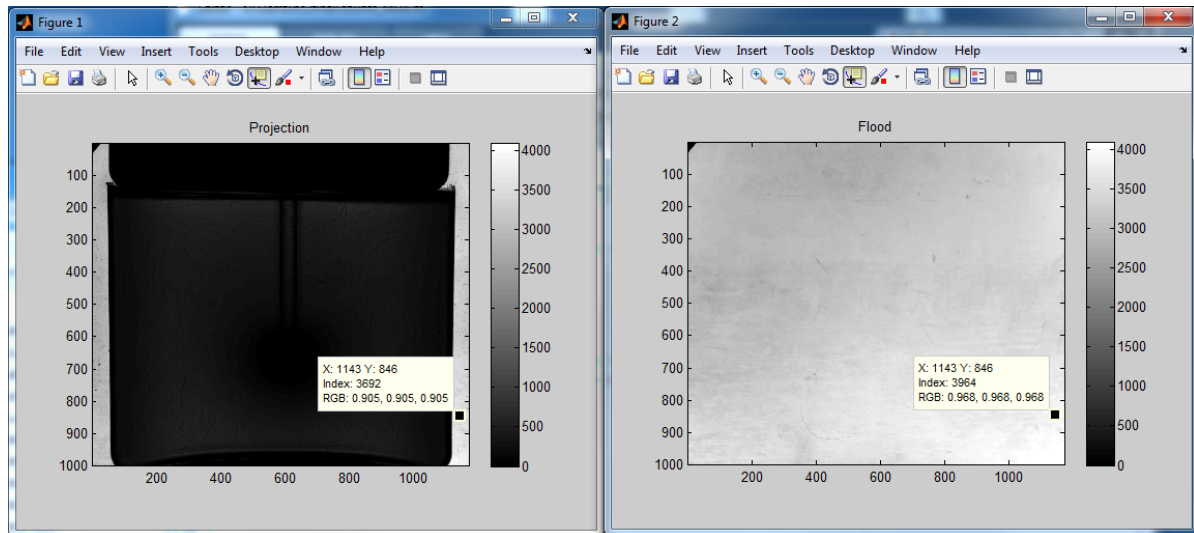


Figure 300. Projection image on left with Index 3692. Flood image on right with Index at same location as in projection image of 3964, giving a delta of less than 30.

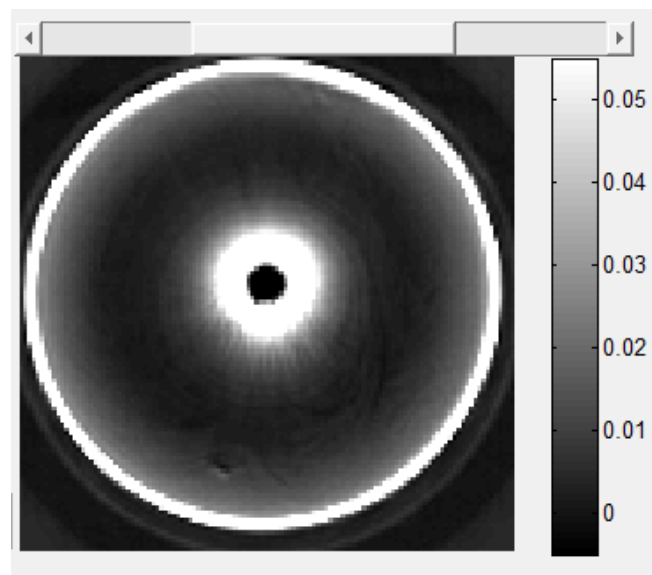


Figure 311. Final post-irradiation scan of a dosimeter showing no ring artifact. The rings seen in this image relate to the dose at various radii.

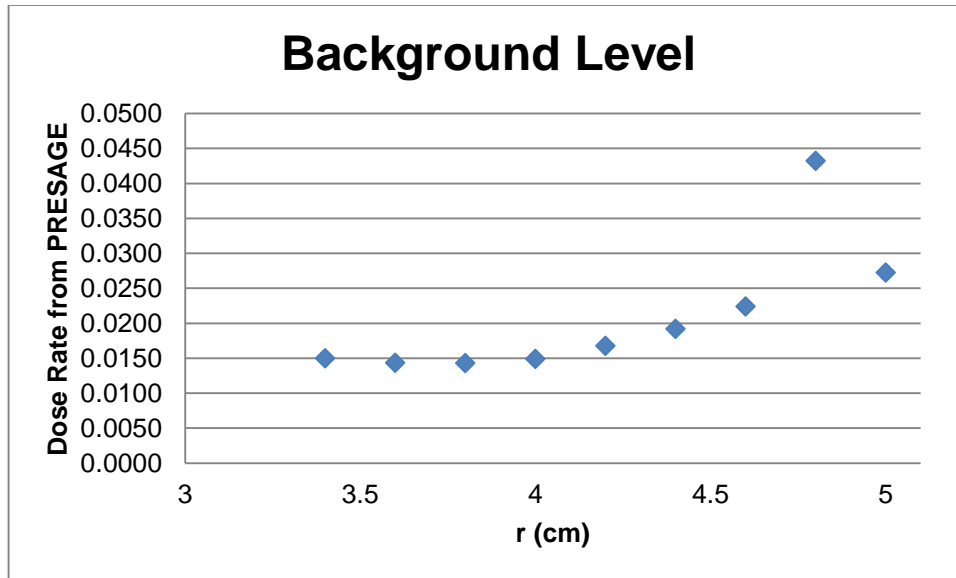


Figure 322. Example background level plot. The background value selected for this dosimeter was 0.0150.

4.2.1 Dose Rate and Dose Rate Constant

Due to this background subtraction correction and the unavailability of applicable cuvette dose calibration curves, the doses reported are relative to each dosimeter. Therefore, the dose rate and dose rate constants were not calculated for comparison.

5 Uncertainty Analysis

TG-43U1 (17) recommends a generic uncertainty analysis for dosimetric quantities measured and calculated for brachytherapy sources. TG-138 (49) outlines a procedure for this analysis. Table 12 contains a summary of Type A ($k=1$) and Type B ($k=1$) uncertainties as well as an estimation of the expanded relative uncertainty ($k=2$), which is defined as a 95% confidence limit. The total standard uncertainty ($k=1$) for the dose rates measured in PRESAGE was estimated to be 5.7%, and the expanded uncertainty ($k=2$) was 11.4%.

The Type A, or statistical, uncertainties in this experiment were all related to the measurements taken in PRESAGE, for both the radial dose function and the anisotropy function. These uncertainties were calculated as the uncertainty in the dose rate at a selected radius (or radius and polar angle) and the uncertainty in the dose rate at the reference point, added in quadrature. The uncertainties in the dose rates were calculated as a percent coefficient of variance. An example for a selected radius and polar angle will be presented in the sections that follow. There were several Type B, or random, uncertainties in this experiment. First, the uncertainty of the air kerma strength measured at the UWADCL includes the equipment used to make the measurement and the

reproducibility of the measurement; this was estimated to be 5% ($k=1$). The uncertainty in the current and voltage supplies used to run the Xofter source was estimated to be less than 1%. Since the anode in the Xofter source is not a point source but has a finite and measureable thickness, this introduces 1.5% uncertainty into the experiment. PRESAGE™ is not exactly water-equivalent, as discussed previously, and so this introduces an estimated 2% uncertainty into the experiment.

The total standard uncertainty is the quadrature sum of all the listed uncertainty components, and the expanded relative uncertainty is simply twice that value.

Uncertainty Component	Type A ($k=1$)	Type B ($k=1$)
Xofter air kerma strength (UWADCL)		5.0%
Current, voltage uncertainty		<1.0%
Anode thickness		1.5%
Water-equivalency of PRESAGE		2.0%
Total standard uncertainty ($k=1$)	5.7%	
Expanded relative uncertainty ($k=2$)	11.4%	

Table 12. Uncertainty in PRESAGE measurement of Dose Rate

5.1 Anisotropy function

The anisotropy function is a ratio between two dose rates. Therefore, uncertainty in the Xofter air kerma strength measurement will cancel out. The uncertainty in current will cancel out as well, leaving the voltage uncertainty as <1%, which will be ignored. The Type A uncertainty at a radius of 3 cm and a polar angle of 60° is 64.4%. This large uncertainty in the measurement dominates the uncertainty estimate for the anisotropy function. Thus, the total uncertainty ($k=1$) for the anisotropy function is 64.4%, and the expanded uncertainty ($k=2$) is 128.9%.

5.2 Radial dose function

The radial dose function is also a ratio of two dose rates, so the Xofter air kerma strength measurement and tube current uncertainties cancel out here as well, and the uncertainty in the voltage can be ignored as before. The Type A uncertainty at a radius of 2 cm is 29.5%. Therefore, the total uncertainty ($k=1$) is 29.6% and the expanded uncertainty ($k=2$) is 59.2%.

6 Conclusion

The hypothesis for this project was rejected. The PRESAGE™ dosimeters were not able to measure, with 95% confidence, the AAPM TG-43U1 dosimetric parameters of the

Xoft Axxent electronic brachytherapy source, to within $\pm 5\%/3\text{mm}$ of Rivard's published values.

Despite errors in methodology, the radial dose and anisotropy functions were more accurate closer to the source. The radial dose function from $r=1\text{ cm}$ to $r=2\text{ cm}$ was within 6% of expected values. The anisotropy function for $\theta=90^\circ \pm 10^\circ$ was within 16% of the accepted values for $r=2\text{ cm}$ and within 10% for $r=3\text{ cm}$. The experiment should be repeated.

To improve this experiment, a new batch of hard dosimeters, containing three of each channel size, should be irradiated using the Xoft source. The pre-irradiation scans, post-irradiation scans, and flood images should all be taken at the same and correct shutter value. Prior to shipping the dosimeters to the UWADCL for irradiations, the pre-irradiation scans should be reconstructed and viewed to ensure the images are "clean" and will provide acceptable data. A dose calibration should be performed by irradiating 10 cuvettes from the same batch as the dosimeters on the 75 kVp orthovoltage machine; the doses delivered should range from 0 Gy to 18 Gy. When irradiating the small channel dosimeters, a dose larger than 15 Gy may be given to ensure the OD at $r = 5\text{ cm}$ is detectable.

As for future work, it would be greatly useful to the lab group, especially future members, to have the cuvette irradiation procedures written out for both orthovoltage and MV linear accelerator machines. The DMOS Scanning Guide should also be updated with a checklist for use during each scan, as well as further explanations on what each scanning parameter controls, how it can be adjusted, and when it should be adjusted. A procedure on how to adjust the matching fluid, including images for comparison, should be written and included in the lab group's training materials. PRESAGE dose calibration data for each batch should be kept in a lab group shared folder for all to reference. The effects of age on a dosimeter, in relation to edge effects, should be further investigated. The two scripts written for this project could be updated to output the standard deviation for the average dose rate calculated for each input dose cube.

This project's findings illustrate the pitfalls of PRESAGE dosimetry, and the need for accurate and thorough training documents. However, PRESAGE remains a viable method to conduct 3D brachytherapy dosimetry, which could greatly improve the understanding of dose distributions for new brachytherapy sources as they are developed, as well as advance quality assurance methods. Future work in dosimetry including the use of brachytherapy applicators in anthropomorphic PRESAGE may begin a new chapter in 3D dosimetry.

Appendix A

Xoft Source TG-43 Parameter Tables (24)

Dose Rate Constant

	Dose Rate Constant (cGy hr ⁻¹ U ⁻¹)
Unfiltered 50 kV source	0.709

Radial Dose Function g(r)

Radius (cm)	Dose Function
0.5	1.418
1.0	1.000
1.5	0.780
2.0	0.641
3.0	0.470
4.0	0.362
5.0	0.286
6.0	0.229
7.0	0.185
8.0	0.150
9.0	0.122
10.0	0.0989
12.0	0.0655
15.0	0.0352

Anisotropy Function F(r, θ)

	Angle (degrees)												
Radius (cm)	0	5	10	15	20	25	30	35	40	45	50	55	60
0.5	0.000	0.000	0.000	0.000	0.000	0.000	0.000	0.252	0.425	0.556	0.676	0.743	0.796
1.0	0.000	0.000	0.000	0.241	0.211	0.211	0.301	0.380	0.483	0.575	0.667	0.738	0.800
1.5	0.000	0.000	0.248	0.267	0.258	0.274	0.361	0.435	0.530	0.609	0.689	0.750	0.811
2.0	0.000	0.000	0.272	0.297	0.298	0.322	0.405	0.476	0.564	0.637	0.709	0.765	0.820
3.0	0.000	0.250	0.296	0.319	0.327	0.357	0.426	0.508	0.590	0.656	0.721	0.773	0.824
4.0	0.000	0.279	0.321	0.343	0.356	0.389	0.450	0.526	0.603	0.665	0.726	0.775	0.825
5.0	0.000	0.290	0.329	0.349	0.364	0.419	0.473	0.545	0.616	0.674	0.731	0.778	0.825

6.0	0.000	0.313	0.349	0.369	0.385	0.424	0.489	0.562	0.626	0.681	0.737	0.782	0.828
7.0	0.000	0.334	0.365	0.383	0.406	0.429	0.504	0.579	0.636	0.692	0.743	0.794	0.830
8.0	0.000	0.349	0.377	0.397	0.420	0.441	0.515	0.589	0.643	0.698	0.747	0.797	0.831
10.0	0.000	0.371	0.395	0.412	0.439	0.459	0.531	0.604	0.657	0.707	0.753	0.800	0.832
12.0	0.000	0.384	0.407	0.426	0.454	0.473	0.542	0.613	0.663	0.712	0.757	0.801	0.831
15.0	0.000	0.401	0.417	0.437	0.465	0.482	0.550	0.622	0.667	0.715	0.758	0.801	0.831

Anisotropy Function $F(r, \theta)$ (continued)

	Angle (degrees)											
Radius (cm)	65	70	75	80	85	90	95	100	105	110	115	120
0.5	0.840	0.883	0.914	0.945	0.970	1.000	1.021	1.041	1.053	1.063	1.065	1.064
1.0	0.840	0.884	0.916	0.948	0.973	1.000	1.020	1.040	1.053	1.065	1.069	1.072
1.5	0.849	0.890	0.920	0.950	0.975	1.000	1.020	1.038	1.052	1.064	1.069	1.074
2.0	0.858	0.895	0.924	0.953	0.977	1.000	1.019	1.037	1.050	1.063	1.069	1.075
3.0	0.860	0.896	0.925	0.954	0.977	1.000	1.019	1.038	1.052	1.065	1.072	1.079
4.0	0.860	0.895	0.924	0.952	0.976	1.000	1.019	1.037	1.050	1.064	1.070	1.077
5.0	0.860	0.894	0.922	0.950	0.975	1.000	1.018	1.036	1.049	1.062	1.069	1.075
6.0	0.862	0.896	0.924	0.952	0.976	1.000	1.019	1.037	1.051	1.064	1.071	1.078
7.0	0.866	0.898	0.929	0.954	0.979	1.000	1.021	1.039	1.056	1.066	1.076	1.081
8.0	0.865	0.898	0.927	0.953	0.979	1.000	1.022	1.039	1.056	1.066	1.076	1.082
10.0	0.866	0.898	0.927	0.952	0.978	1.000	1.021	1.039	1.055	1.066	1.078	1.083
12.0	0.866	0.897	0.926	0.952	0.977	1.000	1.020	1.039	1.056	1.068	1.077	1.089
15.0	0.865	0.895	0.925	0.951	0.977	1.000	1.022	1.039	1.057	1.071	1.083	1.093

Anisotropy Function $F(r, \theta)$ (continued)

	Angle (degrees)											
Radius (cm)	125	130	135	140	145	150	155	160	165	170	175	180
0.5	1.057	1.048	1.028	0.997	0.968	0.944	0.907	0.902	0.893	0.890	0.892	0.887
1.0	1.067	1.062	1.044	1.027	1.005	0.980	0.967	0.960	0.954	0.948	0.947	0.940
1.5	1.072	1.068	1.055	1.042	1.025	1.006	0.998	0.992	0.986	0.980	0.974	0.969
2.0	1.074	1.072	1.062	1.052	1.038	1.024	1.019	1.013	1.007	1.001	0.997	0.993
3.0	1.080	1.080	1.073	1.065	1.054	1.042	1.040	1.037	1.032	1.027	1.023	1.018
4.0	1.079	1.080	1.075	1.070	1.062	1.054	1.051	1.048	1.044	1.041	1.037	1.034
5.0	1.078	1.080	1.078	1.075	1.070	1.065	1.062	1.059	1.057	1.054	1.052	1.050

6.0	1.081	1.083	1.081	1.080	1.077	1.073	1.071	1.069	1.066	1.064	1.064	1.064
7.0	1.086	1.086	1.086	1.085	1.083	1.082	1.080	1.078	1.076	1.075	1.073	1.079
8.0	1.090	1.087	1.088	1.088	1.090	1.084	1.084	1.085	1.080	1.079	1.081	1.080
10.0	1.091	1.091	1.092	1.094	1.097	1.096	1.092	1.092	1.089	1.087	1.093	1.090
12.0	1.094	1.094	1.097	1.098	1.105	1.103	1.101	1.101	1.097	1.097	1.102	1.095
15.0	1.101	1.101	1.105	1.106	1.113	1.111	1.110	1.109	1.107	1.107	1.105	1.110

Appendix B

Radialunicorns.m Code

```
%radialunicorns by sierra
%purpose of this code is currently to spit out average dose/OD values from
%input data cubes at various radii from a center point entered by the user
%for use in TG-43U1 radial dose fcn

clear;
clc;

%input data cube, either manually, or in prompt
% [filename,pathname] = uigetfile('*.mat','PROMPT TEXT HERE');
% load([pathname,filename]);
load('S:\SHARED\Radiation physics\Slade\Top Secret Unicorn Data\8-10-
12Bnew data cube.mat');
%load('C:\Users\jsirwin\Desktop\IMPORTANT DATA CUBES\ss2 data cube.mat');

%enter center coordinates
% cx=0;
% cy=0;
% cz=0;
% cx = input('Enter center x coordinate: ');
% cy = input('Enter center y coordinate: ');
% cz = input('Enter center z coordinate: ');
cx=71;
cy=72;
cz=114;
zsmall=0;
zbig=0;
zsmall=cz-1;
zbig=cz+1;

%enter extent of x, y, z coordinates for use in calculation
% xmax=0;
% ymax=0;
% zmax=0;
% xmax = input('Enter maximum x coordinate: ');
% ymax = input('Enter maximum y coordinate: ');
% zmax = input('Enter maximum z coordinate: ');
xmax=140;
ymax=140;
zmax=151;
```

```

%set real radii to loop through, along with annulus radii (delta from
real)
r=0;
R=0;
delta=0;
radius=[10:2:70]; %radius in mm
num_radii = length(radius); %so can spit out pixelcount & average as
arrays
delta=.5;
r=radius-delta;
R=radius+delta;

%code to ensure that "negative" dose is set to zero dose
Negativeindices=find(ReconstructedSlices.cube<0);
ReconstructedSlices.cube(Negativeindices)=0;

%search for pixels within annulus then adds them up for statistics
analysis
%also computes average value at pixel (sum) for OD/DOSE output
%borrowed from slade's phoenixfire code
Sum=zeros(1,num_radii);
Average=zeros(1,num_radii);
PixelCount=zeros(1,num_radii);
for i=1:num_radii
    for z=zsmall:zbig
        for x=1:xmax
            for y=1:ymax
                if (r(i)<(sqrt((cx-x)^2 + (cy-y)^2)) && (sqrt((cx-x)^2 +
(cy-y)^2)<R(i)))
                    Sum(i)=Sum(i) + ReconstructedSlices.cube(x,y,z);
                    PixelCount(i)=PixelCount(i)+1;
                end
            end
        end
    end
    Average(i)=Sum(i)/PixelCount(i);
end

%this section exports my data to an excel file
%asks where you want to save the excel file, and what to call it
[fileName, pathName]=uiputfile('*.xlsx','Export Profile');
%changes my 3 data arrays into vertical cells & creates one big matrix
data=num2cell([radius; Average; PixelCount]');
%name each column of my data cells
titles = {'Radius', 'Average Dose', 'Pixel Count'};
%place correct title at top of correct data column (cat two things
together)
dataout=cat(1,titles,data);
%writes to the designated file the concatenated matrix i created above
xlswrite(fullfile(pathName,fileName),dataout);

```

Anisotropyunicorns.m Code

```

%anisotropyunicorns by sierra
%purpose of this code is currently to spit out average dose/OD values from
%input data cubes at various radii and angles from a center point entered

```

```

%by the user for use in TG-43U1 anisotropy fcn

clear;
clc;

%input data cube;
%[filename,pathname] = uigetfile('*.mat','Enter data cube file location:
');
% load([pathname,filename]); %to load file from prompt
%load('C:\Users\jsirwin\Desktop\IMPORTANT DATA CUBES\ss2 data cube.mat');
load('S:\SHARED\Radiation physics\Slade\Top Secret Unicorn Data\8-10-
12Bnew data cube.mat');

%enter center coordinates
% cx=0;
% cy=0;
% cz=0;
% cx = input('Enter center x coordinate: ');
% cy = input('Enter center y coordinate: ');
% cz = input('Enter center z coordinate: ');
cx=71;
cy=72;
cz=114;

%enter extent of x, y, z coordinates for use in calculation
% xmax=0;
% ymax=0;
% zmax=0;
% xmax = input('Enter maximum x coordinate: ');
% ymax = input('Enter maximum y coordinate: ');
% zmax = input('Enter maximum z coordinate: ');
xmax=140;
ymax=140;
zmax=151;

%define all my radius, delta, and angle variables outside for loop
theta = [0:10:160];
thetaradians = zeros(size(theta));
radius = [10, 20, 30, 40, 50]; %radius in mm; added 10 for checks, 40 just
b/c
num_radii = length(radius); %get number of radii checking
thetaradians = theta*pi()/180;
num_radian = length(thetaradians); %get number of angles checking
delta = 0;
r = 0;
R = 0;
zsmall=0;
zbig=0;
delta = .5; %in mm

%code to ensure that "negative" dose is set to zero dose
Negativeindices=find(ReconstructedSlices.cube<0);
ReconstructedSlices.cube(Negativeindices)=0;

```

```

%set up variables to be matrices of size radii by angle, for ease of
output
Average=zeros(num_radai,num_radian);
PixelCount=zeros(num_radai,num_radian);
Sum=zeros(num_radai,num_radian);

for radiusloop = 1:num_radai
    for radianloop=1:num_radian

        %define reff in terms of (r, theta)
        reff = radius(radiusloop) * sin(thetaradians(radianloop));

        %calculate delta z from center z coordinate for each reff
        deltaz = radius(radiusloop) * cos(thetaradians(radianloop));

        %apply delta z to center z coordinate correctly
        zeff = cz + deltaz;

        %define inner/outer effective radii
        r = reff - delta;
        R = reff + delta;

        %define z planes to look at. +/-1 seemed like a better choice
        zsmall=round(zeff-1);
        zbig=round(zeff+1);

        %search for pixels within annulus then adds them up for statistics
analysis
        %also computes average value at pixel (sum) for OD/DOSE output
        %borrowed from slade's phoenixfire code
        for z=max(1,zsmall):min(zmax,zbig) %so doesn't go outside cube
coordinates
            for x=1:xmax
                for y=1:ymax
                    if ((r<(sqrt((cx-x)^2 + (cy-y)^2))) && (sqrt((cx-x)^2 +
(cy-y)^2))<R)
                        Sum(radiusloop,radianloop)=Sum(radiusloop,radianloop) +
ReconstructedSlices.cube(x,y,z);
                    end
                end
            end
        end
        Average(radiusloop,
radianloop)=Sum(radiusloop,radianloop)/PixelCount(radiusloop,radianloop);
    end
end

%this section exports my data to an excel file
%asks where you want to save the excel file, and what to call it
[fileName, pathName]=uiputfile('*.xlsx','Export Profile');
%assembling arrays into matrices x 2
dataradius=num2cell(radius');
title={'Radius/Angle'};

```



```

radiusdata=cat(1,title,dataradius);
avgdata=num2cell([theta; Average]);
countdata=num2cell([theta; PixelCount]);
data1=cat(2,radiusdata,avgdata);
data2=cat(2,radiusdata,countdata);
%writes to the designated file & sheet# the 2 matrices i created above
sheet=1;
xlswrite(fullfile(pathName,fileName),data1,sheet);
sheet=2;
xlswrite(fullfile(pathName,fileName),data2,sheet);

```

Appendix C

Radial Dose Function Comparison Data for the Average of all four dosimeters.

r (cm)	Rivard et al. values	PRESAGE values	Standard Deviation	COV (%)	Percent Error
1	1	1	0	0	0
1.2	0.920	1.022	0.354	34.6	11.1
1.4	0.848	1.091	0.564	51.7	28.6
1.6	0.786	1.000	0.656	65.6	27.2
1.8	0.732	0.831	0.614	73.9	13.5
2	0.683	0.688	0.501	72.8	0.7
3	0.511	0.191	0.187	98.0	62.6

References

1. Rivard, M. J., S. D. Davis, L. A. DeWerd, T. W. Rusch, and S. Axelrod. 2006. Calculated and measured brachytherapy dosimetry parameters in water for the Xofigo X-Ray Source: An electronic brachytherapy source. *Medical physics* 33:4020.
2. Webb, S. 2003. The physical basis of IMRT and inverse planning. *British Journal of Radiology* 76:678-689.
3. Niebanck, M., T. Juang, J. Newton, J. Adamovics, Z. Wang, and M. Oldham. 2013. Investigating the reproducibility of a complex multifocal radiosurgery treatment. *Journal of Physics: Conference Series* 444:012072.
4. Azangwe, G., P. Grochowska, D. Georg, J. Izewska, J. Hopfgartner, W. Lechner, C. E. Andersen, A. R. Beierholm, J. Helt-Hansen, H. Mizuno, A. Fukumura, K. Yajima, C. Gouldstone, P. Sharpe, A. Meghzifene, and H. Palmans. 2014. Detector to detector corrections: A comprehensive experimental study of detector specific correction factors for beam output measurements for small radiotherapy beams. *Medical physics* 41:-.
5. Soares, C. G. 2009. Radiochromic Film. 2009 AAPM Summer School.
6. Adamovics, J., and M. J. Maryanski. 2006. Characterisation of PRESAGE: A new 3-D radiochromic solid polymer dosimeter for ionising radiation. *Radiation protection dosimetry* 120:107-112.
7. Huang, O. 2013. Evaluation of PRESAGE® dosimeters for brachytherapy sources and the 3D dosimetry and characterization of the new AgX100 125I seed model. In *Medical Physics/Radiation Physics*. UT Houston Health Sciences Center, UT MD Anderson Cancer Center.
8. Wai, P., J. Adamovics, N. Krstajic, A. Ismail, A. Nisbet, and S. Doran. 2009. Dosimetry of the microSelectron-HDR Ir-192 source using PRESAGE and optical CT. *Applied radiation and isotopes : including data, instrumentation and methods for use in agriculture, industry and medicine* 67:419-422.
9. Holt, R. W., and B. R. Thomadsen. 2012. 3.1 Miniature x-ray tubes will ultimately displace Ir-192 as the radiation sources of choice for high dose rate brachytherapy. In *Controversies in Medical Physics: a Compendium of Point/Counterpoint Debates*. C. G. Orton, and W. R. Hendee, editors. American Association of Physicists in Medicine, College Park, Maryland. 102-106.

10. Dickler, A. 2009. Xofig Axxent electronic brachytherapy: a new device for delivering brachytherapy to the breast. *Nature clinical practice. Oncology* 6:138-142.
11. Dickler, A., M. C. Kirk, A. Coon, D. Bernard, T. Zusag, J. Rotmensch, and D. E. Wazer. 2008. A dosimetric comparison of Xofig Axxent Electronic Brachytherapy and iridium-192 high-dose-rate brachytherapy in the treatment of endometrial cancer. *Brachytherapy* 7:351-354.
12. Rong, Y., and J. S. Welsh. 2010. Surface applicator calibration and commissioning of an electronic brachytherapy system for nonmelanoma skin cancer treatment. *Medical physics* 37:5509.
13. Joiner, M., and A. v. d. Kogel. 2009. *Basic clinical radiobiology*. Hodder Arnold ;, London.
14. Khan, F. M. 2003. *The physics of radiation therapy*. Lippincott Williams & Wilkins, Philadelphia.
15. Hendee, W. R., G. S. Ibbott, and E. G. Hendee. 2005. *Radiation Therapy Physics*. John Wiley & Sons, Inc., Hoboken, NJ.
16. 1985. ICRU Report 38 Dose and Volume Specification for Reporting Intracavitary Therapy in Gynecology. International Commission on Radiation Units and Measurements, Bethesda, Maryland.
17. Rivard, M. J., B. M. Coursey, L. A. DeWerd, W. F. Hanson, M. Saiful Huq, G. S. Ibbott, M. G. Mitch, R. Nath, and J. F. Williamson. 2004. Update of AAPM Task Group No. 43 Report: A revised AAPM protocol for brachytherapy dose calculations. *Medical physics* 31:633.
18. Nath, R., L. L. Anderson, J. A. Meli, A. J. Olch, J. A. Stitt, and J. F. Williamson. 1997. Code of practice for brachytherapy physics: report of the AAPM Radiation Therapy Committee Task Group No. 56. *Medical physics* 24:1557-1598.
19. Goetsch, S. J., F. H. Attix, D. W. Pearson, and B. R. Thomadsen. 1991. Calibration of ¹⁹²Ir high-dose-rate afterloading systems. *Medical Physics* 18:462-467.
20. Kubo, H. D., G. P. Glasgow, T. D. Pethel, B. R. Thomadsen, and J. F. Williamson. 1998. High dose-rate brachytherapy treatment delivery: report of the AAPM Radiation Therapy Committee Task Group No. 59. *Medical physics* 25:375-403.
21. 2011. *Intraoperative Irradiation: Techniques and Results*. Humana Press, Springer Science+Business Media, New York, NY.

22. Ma, C. M., C. W. Coffey, L. A. DeWerd, C. Liu, R. Nath, S. M. Seltzer, and J. P. Seuntjens. 2001. AAPM protocol for 40–300 kV x-ray beam dosimetry in radiotherapy and radiobiology. *Medical physics* 28:868.
23. Park, C. C., S. S. Yom, M. B. Podgorsak, E. Harris, R. A. Price, Jr., A. Bevan, J. Pouliot, A. A. Konski, P. E. Wallner, and G. Electronic Brachytherapy Working. 2010. American Society for Therapeutic Radiology and Oncology (ASTRO) Emerging Technology Committee report on electronic brachytherapy. *International journal of radiation oncology, biology, physics* 76:963-972.
24. 2013. Axxent Electronic Brachytherapy System Operator Manual In Axxent Controller Model 110 Xofter, San Jose, California.
25. Commission, I. E. 2013. Medical electrical equipment. In Part 2-17: Particular requirements for the basic safety and essential performance of automatically-controlled brachytherapy afterloading equipment. IEC, Geneva, Switzerland.
26. Ivanov, O., A. Dickler, B. Y. Lum, J. V. Pellicane, and D. S. Francescatti. 2011. Twelve-month follow-up results of a trial utilizing Axxent electronic brachytherapy to deliver intraoperative radiation therapy for early-stage breast cancer. *Annals of surgical oncology* 18:453-458.
27. Axelrod, S., and T. W. Rusch. 2006. Characterization of MOSFET Response to the Xofter AXXENT X-ray Brachytherapy Source. In 48th AAPM Annual Meeting, Orlando, FL.
28. Chiu-Tsao, S.-T., T. W. Rusch, S. Axelrod, H.-S. Tsao, and L. B. Harrison. 2004. Radiochromic Film Dosimetry for a New Electronic Brachytherapy Source. In 46th AAPM Annual Meeting, Pittsburgh, PA.
29. Rusch, T. W., and M. J. Rivard. 2004. Application of the TG-43 Dosimetry Protocol to Electronic Brachytherapy Sources. In Joint Brachytherapy Meeting GEC/ESTRO - ABS -GLAC, Barcelona, Spain.
30. Rusch, T. W., S. D. Davis, L. A. DeWerd, R. R. Burnside, S. Axelrod, and M. J. Rivard. 2004. Characterization of a New Miniature X-Ray Source for Electronic Brachytherapy. In 46th AAPM Annual Meeting, Pittsburgh, PA.
31. Rusch, T. W., T. D. Bohm, and M. J. Rivard. 2005. Monte Carlo Modeling of the Xofter Axxent X-Ray Source. In 47th AAPM Annual Meeting, Seattle, WA.
32. Taylor, R. E. P., G. Yegin, and D. W. O. Rogers. 2006. Monte Carlo Modeling of the Xofter Axxent X-Ray Source. In 48th AAPM Annual Meeting, Orlando, FL.

33. Gore, J. C., M. Ranade, M. J. Maryanski, and R. J. Schulz. 1996. Radiation dose distributions in three dimensions from tomographic optical density scanning of polymer gels: I. Development of an optical scanner. *Physics in medicine and biology* 41:2695-2704.
34. Baldock, C., Y. D. Deene, S. Doran, G. Ibbott, A. Jirasek, M. Lepage, K. B. McAuley, M. Oldham, and L. J. Schreiner. 2010. Polymer gel dosimetry. *Phys Med Biol* 55:R1-R63.
35. Adamovics, J., K. Jordan, and J. Dietrich. 2006. PRESAGETM - Development and optimization studies of a 3D radiochromic plastic dosimeter–Part 1. *Journal of Physics: Conference Series* 56:172-175.
36. Gorjiara, T., R. Hill, J.-H. Kim, Z. Kuncic, J. Adamovics, and C. Baldock. 2010. Study of dosimetric water equivalency of PRESAGE® for megavoltage and kilovoltage x-ray beams. *Journal of Physics: Conference Series* 250:012053.
37. Guo, P. Y., J. A. Adamovics, and M. Oldham. 2006. Characterization of a new radiochromic three-dimensional dosimeter. *Medical physics* 33:1338.
38. Thomas, A., and M. Oldham. 2010. Fast, large field-of-view, telecentric optical-CT scanning system for 3D radiochromic dosimetry. *Journal of physics. Conference series* 250:1-5.
39. Grant, R. 2011. Optical-CT Scanning Guide. UT MD Anderson Cancer Center.
40. Guo, P., J. Adamovics, and M. Oldham. 2006. A practical three-dimensional dosimetry system for radiation therapy. *Medical physics* 33:3962.
41. Bushberg, J. T., J. A. Seibert, J. Edwin M. Leiboldt, and J. M. Boone. 2002. *The Essential Physics of Medical Imaging*. Lippincott Williams & Wilkins, Philadelphia, PA.
42. 2014. iradon: Inverse Radon Transform. In R2014a Documentation. The Mathworks, Inc. MATLAB.
43. Oldham, M., H. Sakhalkar, P. Guo, and J. Adamovics. 2008. An investigation of the accuracy of an IMRT dose distribution using two- and three-dimensional dosimetry techniques. *Medical physics* 35:2072.
44. Sakhalkar, H., D. Sterling, J. Adamovics, G. Ibbott, and M. Oldham. 2009. Investigating the Feasibility of 3D Dosimetry in the RPC IMRT H&N Phantom. *J Phys Conf Ser* 164:12058.
45. Clift, C., A. Thomas, J. Adamovics, Z. Chang, I. Das, and M. Oldham. 2010. Toward acquiring comprehensive radiosurgery field commissioning data using the

- PRESAGE/optical-CT 3D dosimetry system. *Physics in medicine and biology* 55:1279-1293.
46. Oldham, M., A. Thomas, J. O'Daniel, T. Juang, G. Ibbott, J. Adamovics, and J. P. Kirkpatrick. 2012. A quality assurance method that utilizes 3D dosimetry and facilitates clinical interpretation. *International journal of radiation oncology, biology, physics* 84:540-546.
 47. Oldham, M., and L. Kim. 2004. Optical-CT gel-dosimetry II: Optical artifacts and geometrical distortion. *Medical physics* 31:1093.
 48. Campbell, W. G., D. A. Rudko, N. A. Braam, D. M. Wells, and A. Jirasek. 2013. A prototype fan-beam optical CT scanner for 3D dosimetry. *Medical physics* 40:061712.
 49. DeWerd, L. A., G. S. Ibbott, A. S. Meigooni, M. G. Mitch, M. J. Rivard, K. E. Stump, B. R. Thomadsen, and J. L. M. Venselaar. 2011. A dosimetric uncertainty analysis for photon-emitting brachytherapy sources: Report of AAPM Task Group No. 138 and GEC-ESTRO. *Medical physics* 38:782.

Jennifer Sierra Irwin was born in Idaho Falls, Idaho, on November 5, 1984, the daughter of Claudia Davidson Irwin and Steven Michael Irwin. After completing her dual Bachelor of Science degrees in Physics and Astronomy at The University of Texas at Austin in 2007, she worked as an Ascent Abort Flight Design engineer for United Space Alliance until the space shuttle program ended in 2011. She entered the Medical Physics program at the University of Texas-Houston MD Anderson Cancer Center in August 2012. She completed her research project and the Specialized Master's Degree in Medical Physics in June 2014.

Permanent address:

442 South Main Street

Paris, TX 75460

Email:

sierra.irwin@gmail.com